Modeliranje atmosferskog graničnog sloja u klimatskom zračnom tunelu

Ribičić, Matko

Master's thesis / Diplomski rad

2015

Degree Grantor / Ustanova koja je dodijelila akademski / stručni stupanj: **University of Zagreb, Faculty of Mechanical Engineering and Naval Architecture / Sveučilište u Zagrebu, Fakultet strojarstva i brodogradnje**

Permanent link / Trajna poveznica: https://urn.nsk.hr/urn:nbn:hr:235:977173

Rights / Prava: In copyright / Zaštićeno autorskim pravom.

Download date / Datum preuzimanja: **2024-04-25**

Repository / Repozitorij:

Repository of Faculty of Mechanical Engineering and Naval Architecture University of Zagreb

UNIVERSITY OF ZAGREB
FACULTY OF MECHANICAL ENGINEERING AND NAVAL ARCHITECTURE

MASTER'S THESIS

Matko Ribičić

Zagreb, 2015.

UNIVERSITY OF ZAGREB
FACULTY OF MECHANICAL ENGINEERING AND NAVAL ARCHITECTURE

ATMOSPHERIC BOUNDARY LAYER MODELING IN THE CLIMATIC WIND TUNNEL

Mentors:

Prof. Hrvoje Kozmar, PhD
Prof. Stanislav Pospíšil, PhD

Student:

Matko Ribičić

Zagreb, 2015.

I declare that this thesis was written by myself using knowledge acquired during my study and from the listed literature.

Matko Ribičić

ACKNOWLEDGEMENTS

First of all I would like to express my sincerest gratitude to my mentors Prof. Hrvoje Kozmar and Prof. Stanislav Pospíšil for their enthusiasm, patience and invaluable advice that I have received from them while writing this thesis and during my stay at the Centre of Excellence Telč, Czech Republic. Their company, words of support, and positive attitude have helped me in writing and finishing this thesis for which I am extremely grateful. I could not have imagined having better mentors.

Beside my mentors, I would like to thank my supervisor in the wind tunnel Prof. Sergey Kuznetsov for his guidance and help without whom the experiments in the wind tunnel could not have been possible. My sincere thanks go out to my colleagues Andrija Buljac and Arsenii Trush for their assistance and friendship during my stay at the Centre of Excellence Telč as well as to the technical staff: Pavel Ondrák, Pavel Chvátal and Radek Čábel.

I am thankful to my colleagues from the Faculty of Mechanical Engineering and Naval Architecture for the friendships and memories we have created together at the faculty and to my best friends who have always been there for me through thick and thin.

Finally, I would like to express my eternal gratitude to my family for their unconditional love and support throughout my entire studies and especially to my brother for being the voice of reason when I needed one.

This thesis was supported in part by the Institute of Theoretical and Applied Mechanics of the Academy of Science of the Czech Republic.

Matko Ribičić

SVEUČILIŠTE U ZAGREBU
FAKULTET STROJARSTVA I BRODOGRADNJE
Središnje povjerenstvo za završne i diplomske ispite
Povjerenstvo za diplomske ispite studija strojarstva za smjerove:
procesno-energetski, konstrukcijski, brodostrojarski i inženjersko modeliranje i računalne simulacije

Sveučilište u Zagrebu Fakultet strojarstva i brodogradnje	
Datum	Prilog
Klasa:	
Ur.broj:	

DIPLOMSKI ZADATAK

Student: **Matko Ribičić** Mat. br.: 0035178225

Naslov rada na hrvatskom jeziku: **Modeliranje atmosferskog graničnog sloja u klimatskom zračnom tunelu**

Naslov rada na engleskom jeziku: **Atmospheric boundary layer modeling in the climatic wind tunnel**

Opis zadatka:

Climatic Wind Tunnel (CWT) is a custom-designed and unique facility that allows for experimental simulations of the thermally stratified atmospheric boundary layer (ABL) flow and turbulence including precipitation and icing, as well as their effects on engineering structures and vehicles. Prior to testing of wind effects on engineering structures, it is necessary to model the ABL characteristics in an empty wind-tunnel test section, i.e. without structural experimental models.

In this work, the ABL simulations are to be carried in the newly developed CWT of the Centre of Excellence Telč (CET) in Czech Republic. The influence of individual elements of the Counihan method for the ABL wind-tunnel simulation (castellated barrier wall, vortex generators, surface roughness elements) on the mean flow velocity, turbulence intensity, turbulence length scales, and power spectral density of velocity fluctuations, is to be analyzed and presented. A particular focus is on development of the ABL simulation in the longitudinal (main wind) direction, as well as on the lateral uniformity of the ABL simulation.

In this thesis, it is necessary to provide:
1) Introduction with theoretical background of the atmospheric boundary layer,
2) Experimental setup including wind-tunnel design, experimental technique and methodology,
3) Results and discussion,
4) Conclusions.

It is advised to list references used in this work, as well as to acknowledge help and support possibly received during the course of this study.

Zadatak zadan:	Rok predaje rada:	Predviđeni datumi obrane:
24. rujna 2015.	26. studenog 2015.	2., 3. i 4. prosinca 2015.

Zadatak zadao:
Prof. dr. sc. Hrvoje Kozmar
Prof. dr. sc. Stanislav Pospišil

Predsjednica Povjerenstva:
Prof. dr. sc. Tanja Jurčević Lulić

TABLE OF CONTENTS

LIST OF FIGURES

LIST OF TABLES

LIST OF SYMBOLS

Symbol	Unit	Description
c_w	J/kgK	Specific heat of the hot-wire sensor
d	m	Displacement height
f	rad/s	Coriolis parameter
f_m	s^{-1}	Frequency at which S_u is maximal
h	m	Height of object
k_w	-	Eddy wave number
m	kg	Mass
m_w	kg	Mass of hot-wire sensor
t	s	time
u, v, w	m/s	Absolute velocity in the x-, y- and z-direction
$\overline{u}, \overline{v}, \overline{w}$	m/s	Mean velocity in the x-, y- and z-direction
u', v', w'	m/s	Fluctuating velocity components in the x-, y- and z-direction
$\overline{u}_z$	m/s	Mean velocity at height z
$\overline{u}_{ref}$	m/s	Mean reference velocity in the x-direction
u_δ	m/s	Gradient velocity
u_τ	m/s	Friction velocity
x	m	Distance in the longitudinal direction
y	m	Distance in the lateral direction
y_C	m	Distance in the lateral direction, middle of the cross section
y_L	m	Distance in the lateral direction, left-hand side downwind
y_R	m	Distance in the lateral direction, right-hand side downwind
z	m	Distance in the vertical direction
z_0	m	Aerodynamic surface roughness length
$z_{0,m}$	m	Model aerodynamic surface roughness length
$z_{0,p}$	m	Prototype aerodynamic surface roughness length
z_{ref}	m	Reference height
E	V	Voltage of the Wheatstone bridge
F_c	N	Coriolis force
I_u, I_v, I_w	-	Turbulence intensity in the x-, y- and z-direction
I_w	A	Current intensity
L_u^x, L_u^y, L_u^z	m	Longitudinal integral length scale of turbulence in the x-, y- and z-direction
L_v^x, L_v^y, L_v^z	m	Lateral integral length scale of turbulence in the x-, y- and z-direction
L_w^x, L_w^y, L_w^z	m	Vertical integral length scale of turbulence in the x-, y- and z-direction

R_w	Ω	Resistance of the hot-wire sensor
R_u^x	-	Correlation coefficient
Re_R	-	Roughness Reynolds number
S	-	Length scale factor
S_u	m^2/s^2	Turbulent kinetic energy in the x-direction
T	s	Acquisition time
T_a	K	Temperature of unheated sensor wire
T_w	K	Temperature of heated sensor wire
U	m/s	Velocity in the x-direction
X_u	-	Nondimensional frequency
α	-	Power-law exponent
δ	m	Boundary layer thickness
δ_m	m	Model boundary layer thickness
δ_p	m	Prototype boundary layer thickness
ϕ	rad	Angle of latitude
κ	-	Von Kármán constant
ν	m^2/s	Kinematic viscosity of air
ρ	kg/m^3	Density of air
τ	N/m^2	Reynolds shear stress
ω	s^{-1}	Angular velocity of Earth rotation
Φ_{conv}	W	Convective heat flux

SAŽETAK

Eksperimenti su provedeni u klimatskom zračnom tunelu s ciljem određivanja utjecaja nazubljene barijere, generatora vrtloga i podne hrapavosti na karakteristike strujanja zraka i modeliranog atmosferskog graničnog sloja budući da je precizno eksperimentalno modeliranje atmosferskog strujanja zraka i turbulencije u zračnom tunelu glavni preduvjet kod ispitivanje djelovanja vjetra na građevinske objekte i vozila. Provedena su opsežna mjerenja brzine strujanja zraka, tlaka i temperature uz korištenje užarene žice, Prandtl-Pitotove cijevi i termometra. Rezultati mjerenja su prikazani kao profili vremenski osrednjene brzine, intenziteta turbulencije i turbulentnih duljinskih skala, kao i spektralne raspodjele kinetičke energije turbulencije. Poseban naglasak je na razvoju i jednolikosti strujanja zraka na različitim pozicijama u zračnom tunelu, kao i stabilnost simulacije atmosferskog graničnog sloja na poziciji na kojoj se u zračnom tunelu uobičajeno postavljaju i ispituju strukturni modeli. Barijera uzrokuje smanjenje osrednjene brzine strujanja i povećanje turbulencije blizu podloge, generatori vrtloga pospješuju povećanje turbulencije po cjelokupnoj ispitivanoj visini od podloge, dok je povećanje turbulencije i smanjenje brzine strujanja uslijed djelovanja podne hrapavosti ograničeno na sloj neposredno iznad podloge. Uspješno je generiran model atmosferskog graničnog sloja karakterističan za strujanje vjetra i turbulenciju iznad prigradskog/gradskog tipa terena. Mjerilo simulacije atmosferskog graničnog sloja ostvarenog mjerenjima iznosi 1:300, a eksperimentalni rezultati se dobro podudaraju s prethodnim istraživanjima, međunarodnim propisima i standardima. Modelirani atmosferski granični sloj je razvijen i jednolik u uzdužnom i poprečnom smjeru na poziciji na kojoj se uobičajeno postavljaju i ispituju strukturni modeli.

Ključne riječi:

Eksperimentalna aerodinamika okoliša, atmosferski granični sloj, turbulencija, simulacije u zračnom tunelu, Counihanova metoda, mjerenje brzine, tlaka i temperature

PROŠIRENI SAŽETAK

1. Uvod

Atmosferski granični sloj je sloj zraka u blizini Zemljine površine karakteriziran trenjem između zraka i podloge, koji bitno utječe na probleme vezano uz djelovanje vjetra na konstrukcije, disperziju štetnih čestica u atmosferi, energiju vjetra i urbanu mikrometeorologiju. Uobičajeno se ispituje ekperimentalno na meteorološkim tornjevima i na modelima u zračnom tunelu, kao i uz pomoć računalnih simulacija. Nakon izgradnje novog zračnog tunela, a prije mjerenja na strukturnim modelima, potrebno je detaljno ispitati karakteristike strujanja zraka i turbulenciju u zračnom tunelu, kao i karakteristike simulacije atmosferskog graničnog sloja. Cilj ovog rada je eksperimentalno ispitivanje utjecaja nazubljene barijere, generatora vrtloga i podne hrapavosti na karakteristike strujanja zraka i modeliranog atmosferskog graničnog sloja u klimatskom zračnom tunelu Centra izvrsnosti Telč u Češkoj Republici.

2. Atmosferski granični sloj

Strujanje zraka u atmosferskom graničnom sloju je rezultat pretvorbe toplinske energije, uslijed zračenja Sunčevih zraka, u mehaničku energiju. Sile koje djeluju na struju zraka su uzgonska sila kao posljedica temperaturnih razlika, gradijentna sila uslijed razlike tlaka, Coriolisova sila zbog djelovanja Zemljine rotacije, i sila trenja struje zraka i tla.

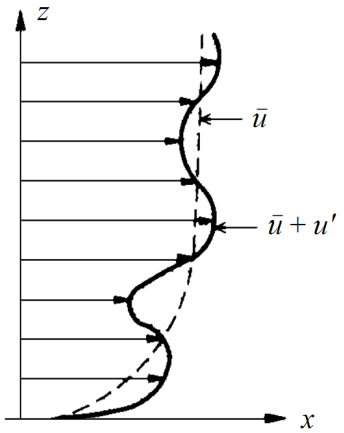

Slika 1 Profil brzine u uzdužnom smjeru s naznačenom apsolutnom i srednjom brzinom

Približna debljina atmosferskog graničnog sloja iznosi između 450 i 600 m, a najznačajnije svojstvo je izražena atmosferska turbulencija s karakterističnim pulzacijama svih fizikalnih veličina, slika 1. Najznačajniji parametri koji opisuju atmosferski granični sloj su srednja brzina struje zraka, intenzitet turbulencije, turbulentne duljinske skale, Reynoldsovo smično naprezanje i spektar kinetičke energije turbulencije.

3. Simuliranje atmosferskog graničnog sloja u zračnom tunelu

Mjerenja u sklopu ovog rada su provedena u klimatskom zračnom tunelu Centra izvrsnosti Telč u Češkoj Republici. Mjerenja brzine su provedena metodom užarene žice uz pomoć anemometra konstantne temperature. Osnovni princip rada užarene žice je izmjena topline između žice i zraka koji nastrujava, pri čemu se temperatura žice održava konstantnom.

Postoji nekoliko metoda koje se koriste za simuliranje atmosferskog graničnog sloja u zračnom tunelu, od kojih je najzastupljenija Counihanova metoda. Ova metoda se uobičajeno primjenjuje u zračnim tunelima za generiranje graničnog sloja s kratkom mjernom sekcijom, a osnovni elementi su nazubljena barijera, generatori vrtloga i podna hrapavost, slika 2.

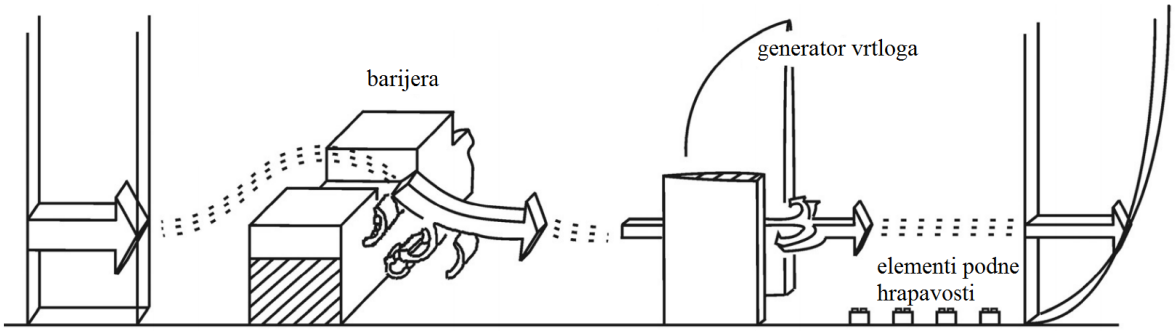

Slika 2 Princip simulacije atmosferskog graničnog sloja u zračnom tunelu uz primjenu Counihanove metode

Strujanjem zraka preko barijere nastaju vrtlozi s horizontalnom osi vrtnje u poprečnom smjeru u odnosu na smjer glavnog strujanja. Generatori vrtloga potiču nastajanje vrtloga s vertikalnom osi vrtnje. Podna hrapavost omogućava fino modeliranje turbulencije zraka u neposrednoj blizini podloge i održavanje strukture modeliranog atmosferskog graničnog sloja.

4. Rezultati i zaključak

Eksperimentalni rezultati su prikazani kao vremenski osrednjene brzine, intenzitet turbulencije, turbulentne duljinske skale i spektralna raspodjela kinetičke energije turbulencije. Analiziran je utjecaj pojedinih elemenata Counihanove metode na karakteristike strujanja i turbulencije struje zraka, i modeliranog atmosferskog graničnog sloja, slike 3 do 6.

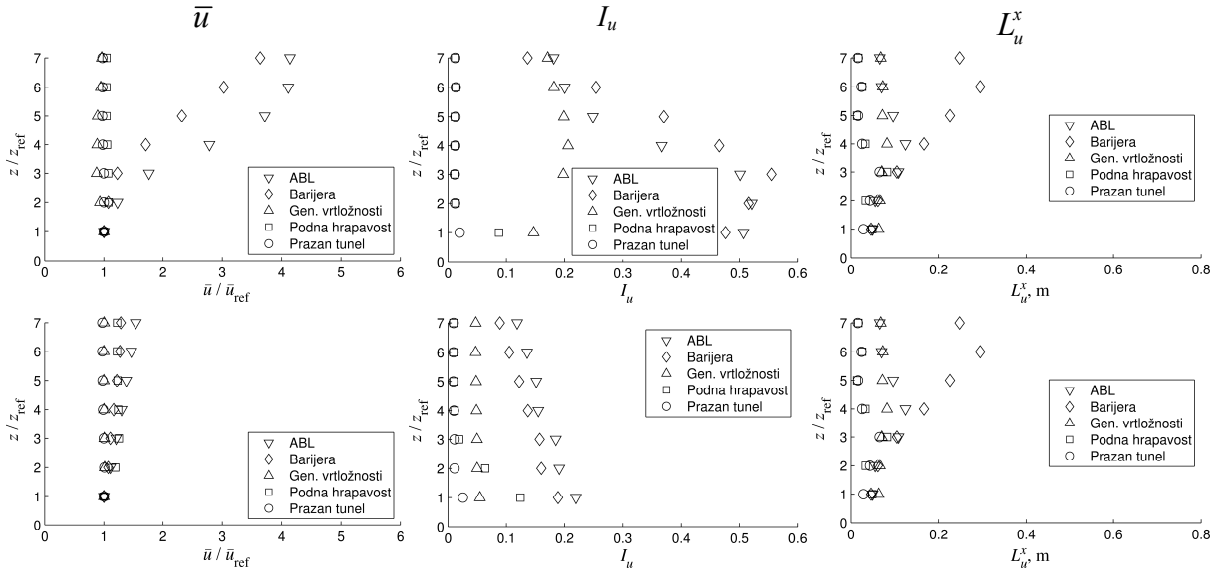

Slika 3 Utjecaj elemenata Counihanove metode na profile srednje brzine, intenziteta turbulencije te duljinskih mjera turbulencije; prvi red su rezultati na ulazu u mjernu sekciju, drugi red su rezultati na poziciji na kojoj na poziciji na kojoj se uobičajeno postavljaju i ispituju strukturni modeli; prvi stupac su osrednjene brzine strujanja, drugi stupac intenzitet turbulencije, treći stupac turbulentne duljinske skale

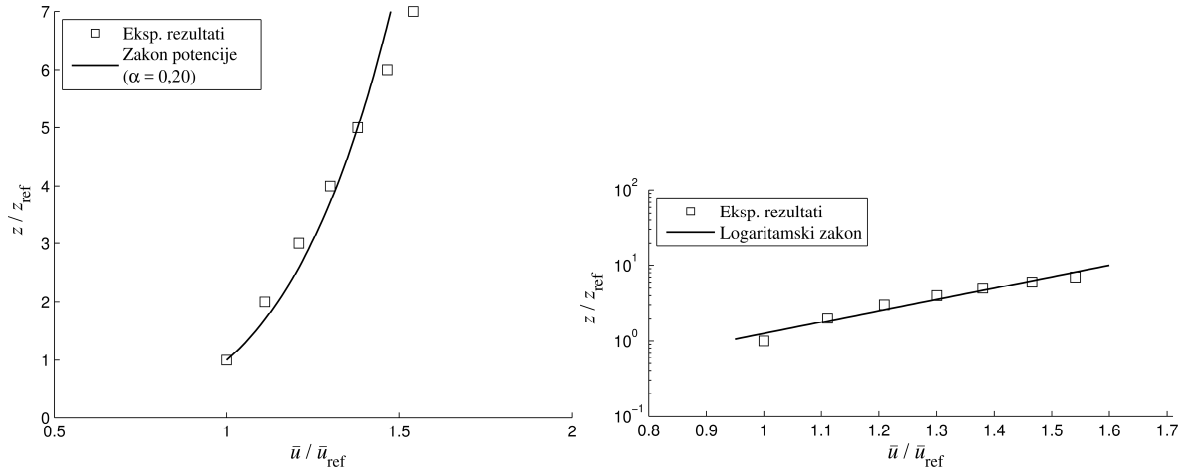

Slika 4 Usporedba profila osrednjenih vrijednosti brzine sa zakonom potencije (lijevo) i logaritamskim zakonom (desno)

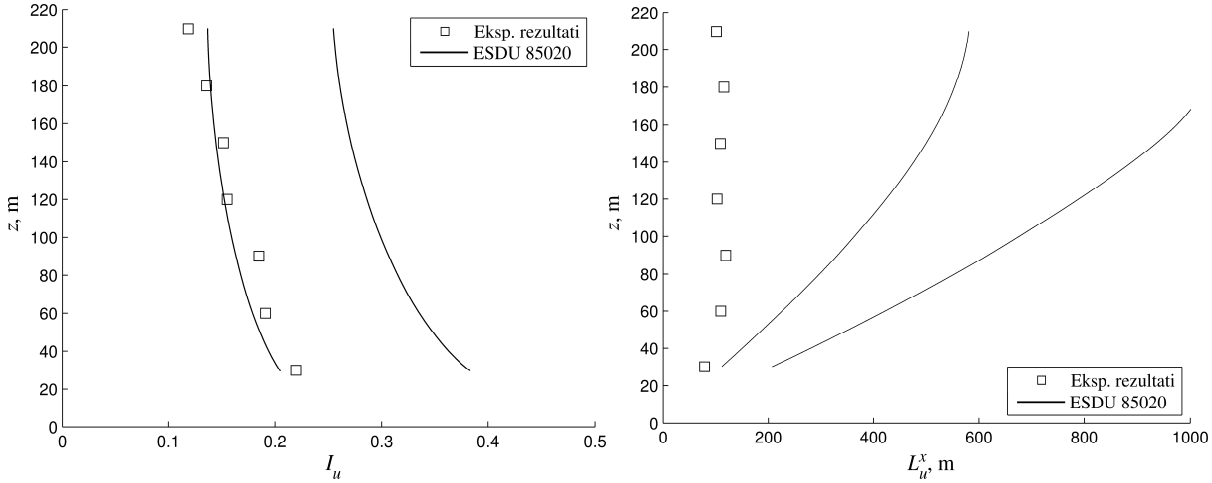

Slika 5 Usporedba profila intenziteta turbulencije (lijevo) i duljinskih mjera turbulencije (desno) s međunarodnim standardom ESDU 85020

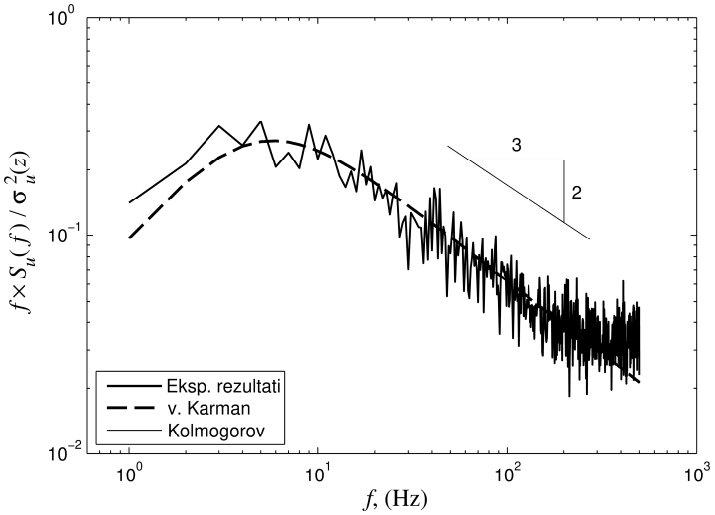

Slika 6 Usporedba spektralne raspodjele kinetičke turbulencije s teorijskim modelima von Kármána i Kolmogorova

Barijera uzrokuje smanjenje osrednjene brzine strujanja i povećanje turbulencije blizu podloge, generatori vrtloga pospješuju povećanje turbulencije po cjelokupnoj ispitivanoj visini od podloge, dok je povećanje turbulencije i smanjenje brzine strujanja uslijed djelovanja podne hrapavosti ograničeno na sloj neposredno iznad podloge. Uspješno je generiran model atmosferskog graničnog sloja karakterističan za strujanje vjetra i turbulenciju iznad prigradskog/gradskog tipa terena. Modelirani atmosferski granični sloj je razvijen i jednolik u uzdužnom i poprečnom smjeru na poziciji na kojoj se uobičajeno postavljaju i ispituju strukturni modeli. Mjerilo simulacije atmosferskog graničnog sloja ostvarenog mjerenjima iznosi 1:300, a profil osrednjenih vrijednosti brzine se dobro podudaraju sa zakonom potencije karakteriziran vrijednosti eksponenta 0,20 i logaritamskim zakonomu

neposrednoj blizini podloge. Profili intenziteta turbulencije i turbulentnih duljinskih skala se podudaraju s međunarodnim standardom ESDU 85020 za vrijednosti aerodinamičke duljine hrapavosti 0,1 m. Spektralna raspodjela kinetičke energije turbulencije eksperimentalnih rezultata se podudara s teorijskim modelima von Kármána i Kolmogorova.

SUMMARY

Experiments are carried out in the climatic wind tunnel to investigate the influence of castellated barrier wall, vortex generators and surface roughness on flow characteristics and the simulated atmospheric boundary layer, as precise modeling of atmospheric flow and turbulence in the wind tunnel is a key prerequisite when studying wind effects on structures and vehicles. Extensive measurements were carried out to determine flow velocity, pressure and temperature using hot wire, Prandtl-Pitot tube, pressure sensors and thermometers. Experimental results were reported as profiles of mean flow velocity, turbulence intensity and turbulent length scales, as well as power spectral density of velocity fluctuations. A particular focus was on flow development and uniformity at various positions in the wind-tunnel test section, as well as characteristics of the atmospheric boundary layer simulations at the turntable. The barrier was observed to cause a decrease in flow velocity and an increase in the turbulence close to the surface, vortex generators enhance turbulence throughout the entire height range under scope, while an increased turbulence and a decreased flow due to surface roughness is exhibited close to surface. The atmospheric boundary layer is successfully simulated for suburban/urban type of terrain. The simulation length scale is 1:300. Experimental results are in good agreement with previous studies, international standards and codes. The simulated atmospheric boundary layer is developed and uniform at the turntable.

Key words:

Experimental environmental aerodynamics, Atmospheric boundary layer, Turbulence, Wind-tunnel experiments, Counihan method, Velocity, pressure and temperature measurements

1. INTRODUCTION

The interest in wind tunnel simulations of the atmospheric boundary layer (ABL) has been increasing since the second part of the 20th century. ABL is a region of air in the lowest part of the atmosphere, which is greatly influenced by Earth surface. The ABL considerably influences various issues with respect to wind effects on structures, air pollution dispersion and dilution, wind energy and urban micrometeorology. It is commonly studied using field measurements, wind-tunnel experiments and computational simulations.

The problem using field measurements is that the weather conditions cannot be fully controlled and the measurements can be done on completed structures only. Computational simulations provide a complete picture of flow characteristics in the computational domain, but are less reliable with respect to turbulence characteristics. Although the reliability and precision of numerical simulations has been increased and they present a less expensive option than field- and wind-tunnel tests, the simulation of turbulence is considered more important and essential which is an advantage of wind-tunnel experiments.

Once a new boundary layer wind tunnel (BWLT) is built, like recently the climatic wind tunnel in the Centre of Excellence Telč (CET), Czech Republic, it is necessary to investigate its flow characteristics prior to performing experiments on structural models. The preliminary measurements commonly include evaluation of the ABL simulations as well. The basic idea of ABL simulation in a wind tunnel is to install a combination of objects and force the flow to simulate flow and turbulence similar to the atmospheric conditions.

The results of wind-tunnel ABL simulations are expected to correctly model flow and turbulence developing above various types of terrain, e.g. urban, suburban or rural terrain. This can be arranged using various experimental setups of simulation hardware. One of the commonly adopted simulation methods is the Counihan method that uses a castelated barrier wall, vortex generators and surface roughness to simulate the ABL at simulation length scales from 1:100 to 1:1000.

In this work, the ABL simulations were carried out in the newly developed climatic wind tunnel of the Centre of Excellence Telč (CET) in Czech Republic. The influence of individual elements of the Counihan method for the ABL wind-tunnel simulation (castellated barrier wall, vortex generators, surface roughness elements) on the mean flow velocity, turbulence

intensity, turbulence length scales, and power spectral density of velocity fluctuations was analyzed. A particular emphasis was on flow and turbulence development and uniformity, as well as on characteristics of the created ABL simulation. An introduction with a theoretical background of the ABL, experimental setup including wind-tunnel design, experimental technique and methodology are provided. Experimental results are compared with previous studies, commonly adopted theoretical and empirical laws, international standards and codes.

2. WIND-TUNNEL SIMULATION OF THE ATMOSPHERIC BOUNDARY LAYER

2.1. Atmospheric flow and turbulence

Flow in the atmosphere is a set of complex phenomena and atmospheric motion is characterized by different patterns of motion that are mutually independent both in time and space. Figure 2.1 shows that the patterns of atmospheric motion range from turbulence (vortices of air in the range of a few meters with a characteristic lifetime of some minutes) to local weather systems and large planetary waves, which may circumvent the entire globe and have a lifetime of several days. These phenomena are referred to as microscale, convective scale and macroscale, respectively [1].

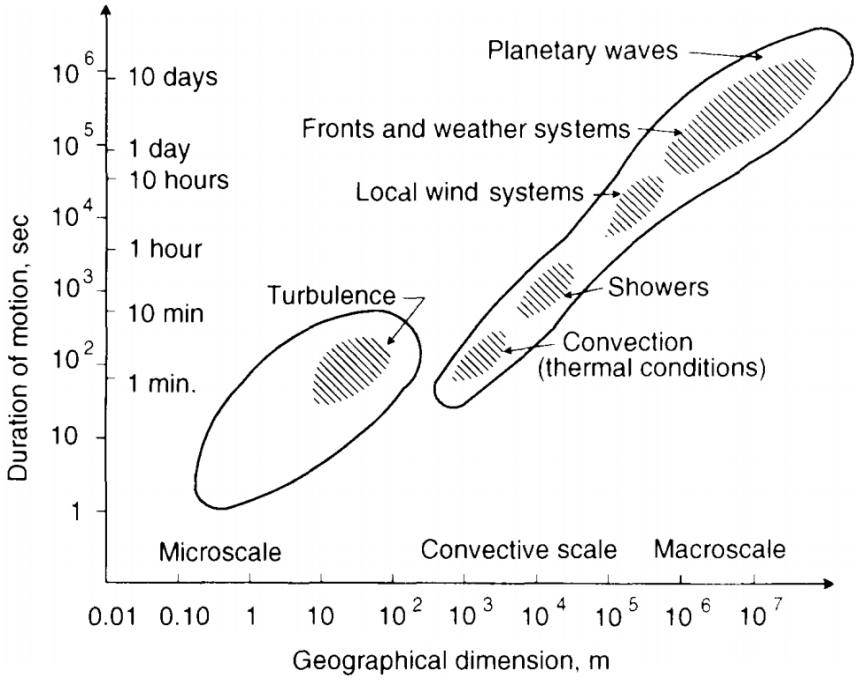

Figure 2.1 Orders of magnitude in space and time for different patterns of motion in the atmosphere, Dyrbye and Hansen [1]

The flow of air in the atmosphere is known as wind and it arises as a result of pressure differences in the atmosphere. The wind itself also causes considerable changes in the atmospheric pressure and vice versa [1].

2.1.1. Equilibrium of forces

The motion of air is governed by vertical and horizontal forces. The vertical force that drives the particles of air is the vertical buoyancy force and, depending on the vertical temperature distribution, the buoyancy force acts upwards, downwards or is zero. These three cases correspond to unstable, stable or neutral atmospheric stratification, respectively. Figure 2.2 shows wind profiles in stable, neutral and unstable air [2].

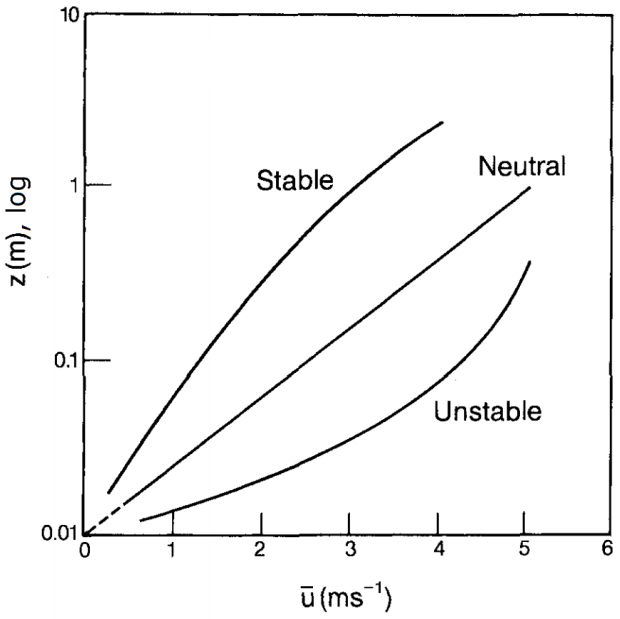

Figure 2.2 Wind profile in stable, neutral and unstable air, Kaimal and Finnigan [2]

On the other hand, the horizontal pressure gradient force, the Coriolis force and the force of friction are the forces that govern the motion of air in the horizontal direction. The cause of the horizontal pressure gradient force is the difference in pressure in the horizontal direction. If a point is observed on an isobar, i.e. on a line of constant pressure (as shown in Figure 2.3 [1]), the force is perpendicular and is directed from high-pressure to low-pressure regions. The term which describes the pressure gradient force is:

$$P = \frac{1}{\rho}\frac{\mathrm{d}p}{\mathrm{dn}}, \tag{2.1}$$

where ρ is the density of air. Due to Earth rotation and the inertia of air, to an observer on Earth it appears as if the path describing a particle of air is curved. The deviation is caused by the Coriolis force, which is equal to:

$$F_c = mfv, \tag{2.2}$$

where m is the mass of the particle and v is the velocity of the particle. The Coriolis parameter f is defined as:

$$f = 2\omega \sin\phi, \tag{2.3}$$

where $\omega = 0.7292 \times 10^{-4}$ s^{-1} is the angular velocity of Earth rotation and ϕ is the angle of latitude. The Coriolis force acts in a direction perpendicular to the rotation axis and to the velocity of the body in the rotating frame.

Friction near the Earth surface is the main cause of a decrease in wind velocity. This horizontal drag force or the friction force decreases with height because the influence of friction decreases and beyond a certain height, called the gradient height, becomes negligible.

Wind is the result of equilibrium between the pressure gradient force, the Coriolis force and the friction force, Figure 2.3 [1] .

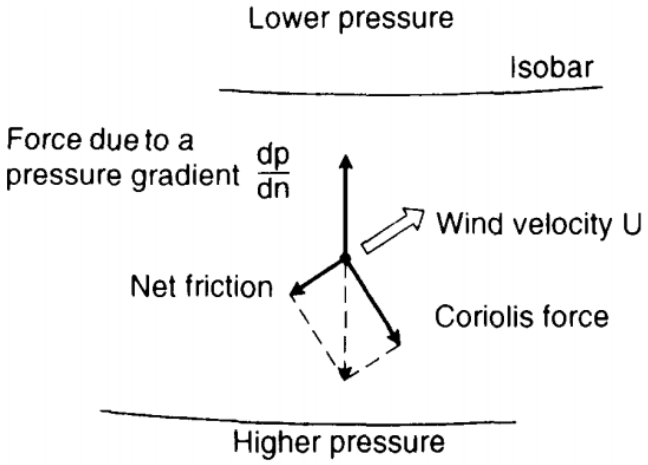

Figure 2.3 Equilibrium of forces in the atmosphere, Dyrbye and Hansen [1]

Due to friction, the velocity at the surface is equal to zero and it increases with increasing height. The Coriolis force, which is proportional to the velocity, increases with height as well. The combined effect of the friction and the Coriolis force is manifested in the angle between the direction of motion and the isobars which increases from zero at the gradient height to its largest value at the Earth surface. The structure of the wind from the Earth surface to the gradient height, i.e. throughout the atmospheric boundary layer, is represented by the Ekman spiral, Figure 2.4 [1].

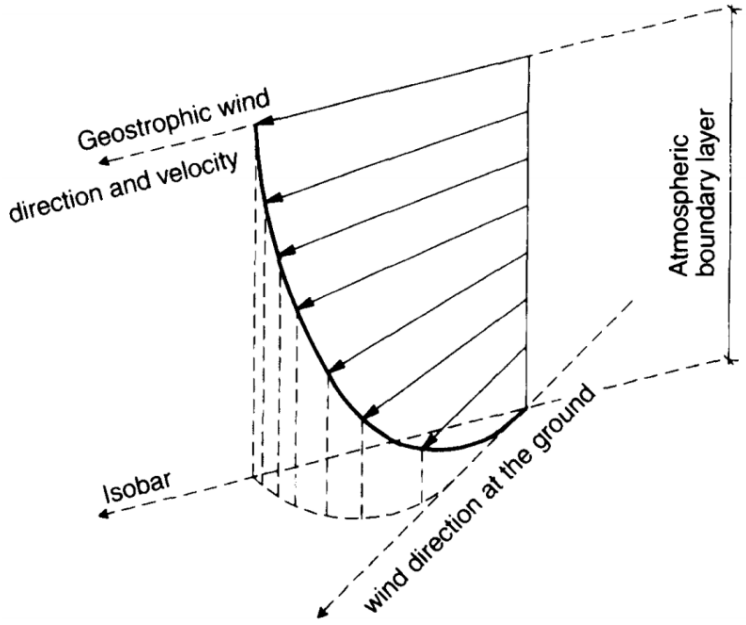

Figure 2.4 Ekman spiral in the atmospheric boundary layer, Dyrbye and Hansen [1]

2.1.2. Atmospheric turbulence

Turbulence in the wind is caused by dissipation of the wind kinetic energy into thermal energy via creation and destruction of progressively smaller eddies (or gusts). Turbulent wind may have a relatively constant mean velocity over time periods of an hour or more, but over shorter times (minutes or less) it may be quite variable, Figure 2.5 [3]. The basic nature of turbulent flow is that the describing parameters are not constant with respect to time at fixed points in space and they fluctuate through a wide range of frequencies. Motion is chaotic, particles move randomly and it is difficult to describe temperature, pressure, density and humidity as well as the motion of air itself, as small changes in initial conditions may induce large differences in the later estimations [1].

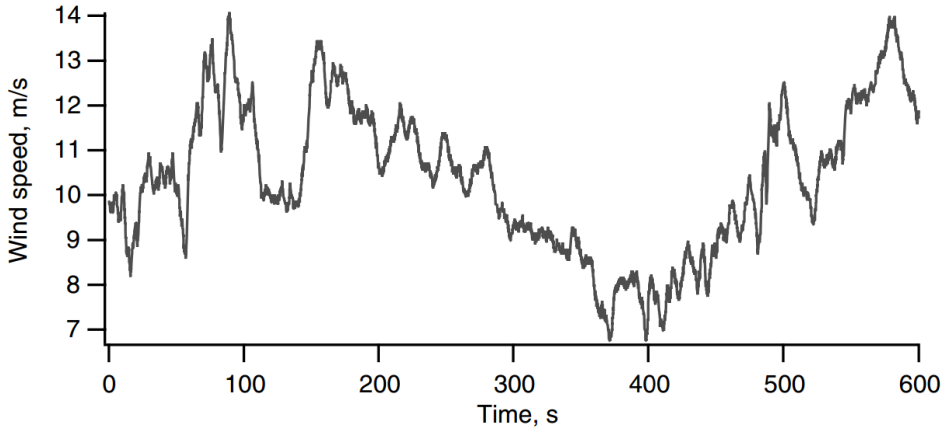

Figure 2.5 Sample time history of wind velocity, Manwell, McGowan and Rogers [3]

Simiu and Scanlan [4] indicate that when accurately describing the ABL, it is also important to describe its characteristics such as turbulence intensity and turbulent length scales, as well as their variation with height, and the spectra of turbulence.

2.2. Atmospheric boundary layer

The ABL is the lowest part of the troposphere, the region most directly influenced by an exchange of momentum, heat, and water vapor at the Earth surface. Turbulent motions on time scales of an hour or less dominate the flow in this region, transporting atmospheric properties both horizontally and vertically. The mean properties of the flow in this layer (the wind speed, temperature, and humidity) exhibit strongest gradients in the lowest 50 m to 100 m. Turbulent exchange in this shallow layer controls the exchange of heat, mass, and momentum at the surface and thereby the conditions in the entire ABL [2].

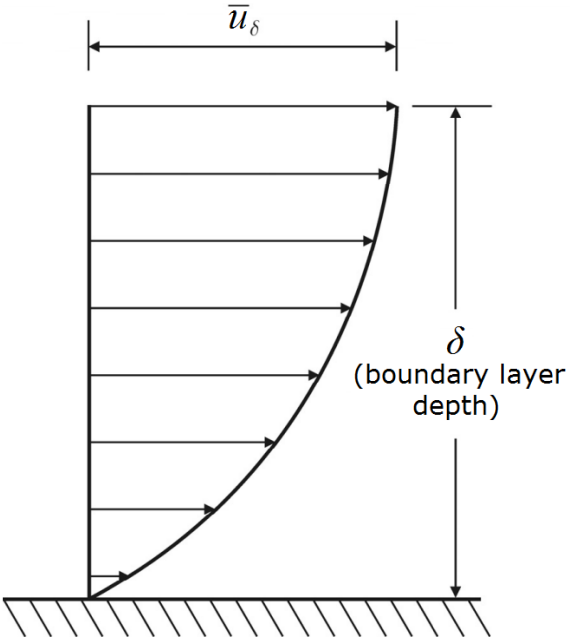

Figure 2.6 Atmospheric boundary layer, Kozmar [5]

The height at which the velocity is maximum is called the boundary layer thickness δ and the velocity at that height is called gradient velocity u_δ, Figure 2.6 [5]. Atmosphere above the boundary layer thickness δ is called the free atmosphere.

2.2.1. ABL structure

According to Counihan [6], the mean height of the atmospheric boundary layer above both urban and rural landscape is between 450 and 600 m. It is divided into two distinctive regions: the inner layer, which consists of the interfacial and inertial sublayer, and the outer layer. Figure 2.7 [5] shows the structure of the ABL, where δ is the height of the boundary layer, z is the height above ground and z_0 is the aerodynamic surface roughness length.

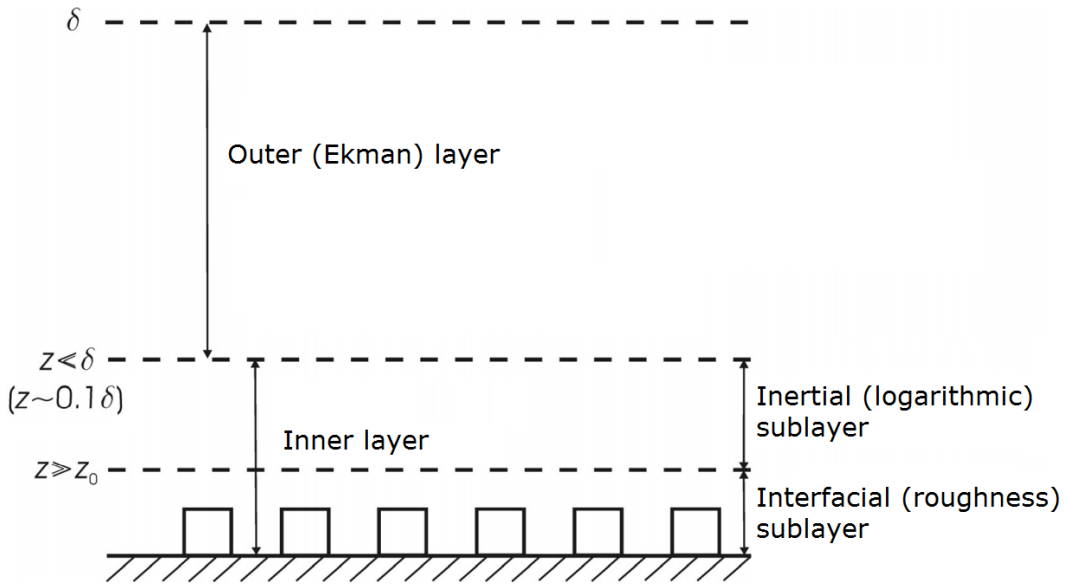

Figure 2.7 Schematic structure of the ABL, Kozmar [5]

The layer close to the surface is the interfacial or roughness sublayer where molecular transport dominates over turbulent transport. Here, the heat exchanges between the surface and the air. Above the interficial sublayer is the inertial sublayer in which the Coriolis forces and the pressure forces can be neglected and the wind has a constant direction while the velocity is horizontal. Together, both of the sublayers form the inner layer that is mainly dependant on the surface characteristics and the height of the inner layer is usually up to 100 m (10-15% of the ABL thickness). On the other hand, the outer layer does not depend on the nature of the surface and it is more affected by the Earth rotation, i.e. by the Coriolis force. It is also called the Ekman layer, since Ekman (1905) first studied the rotation effects on boundary layer flow in the ocean. The transition between the inner and the outer layer is not abrupt because there is an overlap region between them [5].

2.2.2. Mean velocity characteristics

2.2.2.1. Reynolds averaging

The flow in the ABL is very turbulent, as the wind velocity considerably fluctuates around its mean value, Figure 2.8 [1]. When simulating the ABL it is important to take into consideration the fluctuations that occur in the atmosphere in addition to the mean wind velocity.

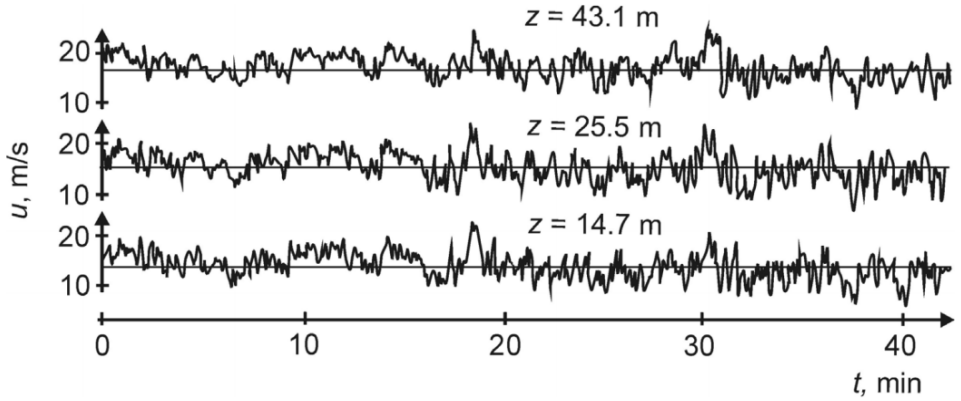

Figure 2.8 Sample time history of wind velocity recorded at various heights within the atmospheric boundary layer, Dyrbye and Hansen [1]

In order to differentiate the mean value from the fluctuating component of the absolute (instantaneous) velocity, the absolute velocity is represented as the sum of the mean velocity ($\overline{u}, \overline{v}, \overline{w}$) and the fluctuating (turbulent) component (u',v',w'):

$$u = \overline{u} + u', \qquad \text{for } x\text{-direction (longitudinal)} \tag{2.4}$$

$$v = \overline{v} + v', \qquad \text{for } y\text{-direction (lateral)} \tag{2.5}$$

$$w = \overline{w} + w'. \qquad \text{for } z\text{-direction (vertical)} \tag{2.6}$$

The mean or time-averaged value of velocity is obtained by a procedure called the Reynolds averaging and in the x-direction is equal to:

$$\overline{u} = \frac{1}{T}\int_{-T/2}^{T/2} u(t-T)\,\mathrm{d}t, \tag{2.7}$$

where T is the acquisition time. Figure 2.9 [1], [3] shows an example of a vertical velocity profile, where the solid line and the dotted line represent the absolute and the mean velocity, respectively.

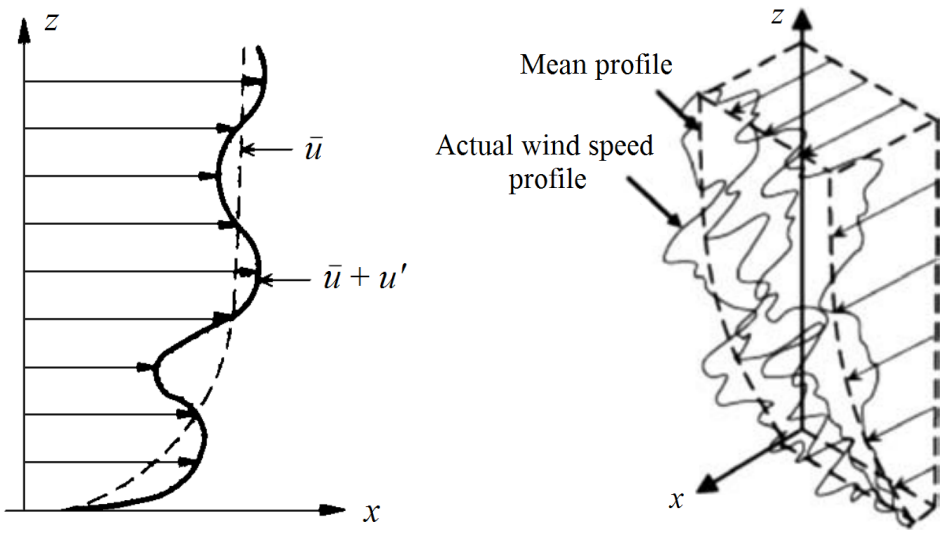

Figure 2.9 Vertical velocity profile of the absolute and the mean wind velocity in the main wind direction, Dyrbye and Hansen [1], Manwell, McGowan and Rogers [3]

Although the ABL flow is three dimensional, the value of the mean velocity in the longitudinal direction is larger than the values of mean velocities in other directions, i.e. $\bar{u} \gg \bar{v}$ and $\bar{u} \gg \bar{w}$. Therefore, $\bar{v}$ and $\bar{w}$ velocity components are commonly neglected when analyzing experimental results from a wind tunnel.

2.2.2.2. Aerodynamic surface roughness length

The mean wind velocity depends not only on the height above the surface, but also on the aerodynamic surface roughness length z_0. The aerodynamic surface roughness length z_0 (Figure 2.11 [1]) is defined as the height above the ground where the wind speed becomes zero due to the effects of vegetation or obstacles. The defining factors of the aerodynamic surface roughness length are the height, shape and spacing density of surface roughness elements. With the increase of the surface roughness, i.e. buildings and similar obstacles, the mean velocity values are decreasing.

Simiu and Scanlan [4] defined typical roughness heights for different terrains:

1. Urban: $2 \text{ m} < z_0 < 3 \text{ m}$
2. Suburban: $0.2 \text{ m} < z_0 < 1.2 \text{ m}$
3. Rural: $0.001 \text{ m} < z_0 < 0.2 \text{ m}$
4. Smooth: $0.001 \text{ m} < z_0 < 0.006 \text{ m}$

The dependence of the aerodynamic surface roughness length z_0 on the structure of the surface roughness is provided in ESDU 82026 [7] as well, Figure 2.10 [7].

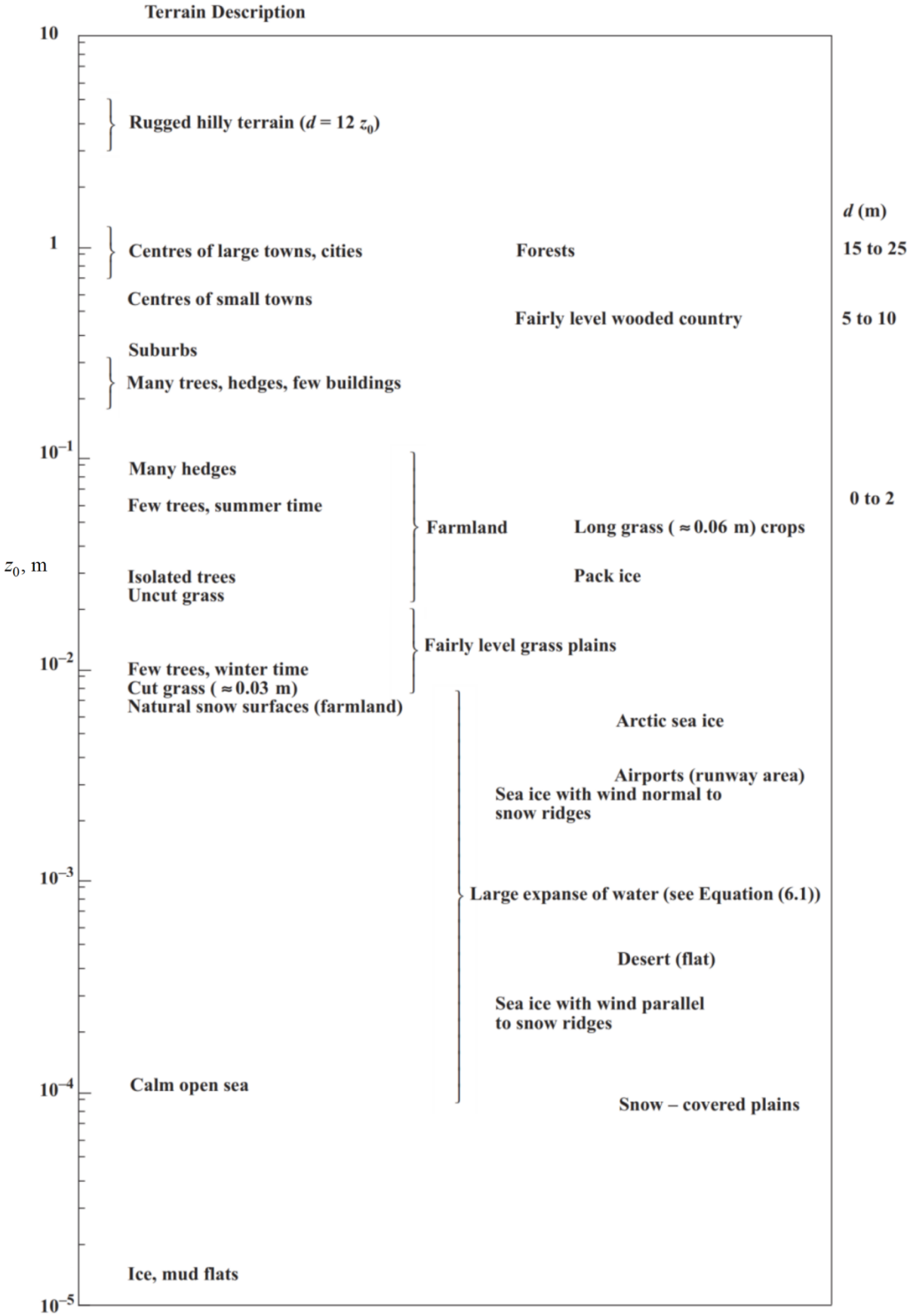

Figure 2.10 Aerodynamic surface roughness length z_0 for various terrain types, ESDU 82026 [7]

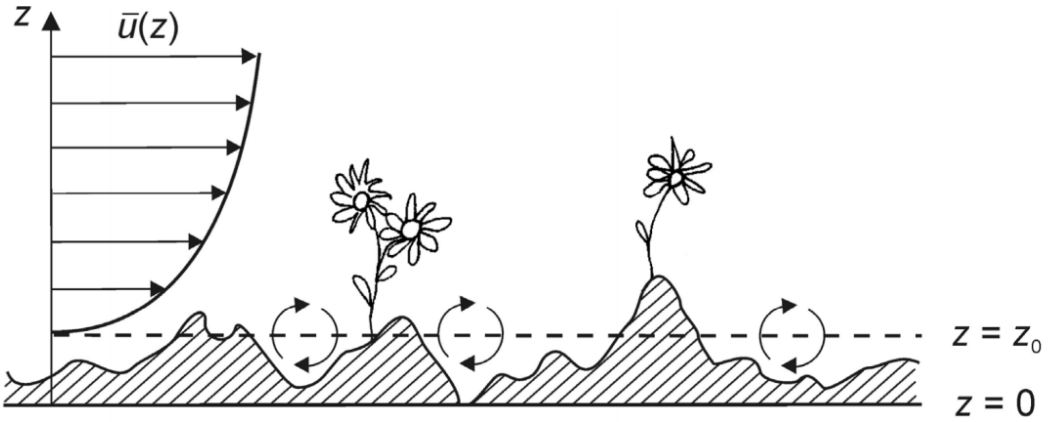

Figure 2.11 Simplified illustration of the aerodynamic surface roughness length z_0, Dyrbye and Hansen [1]

2.2.2.3. Power law

An empirical power law that represents well the vertical velocity profile in the atmosphere was originally suggested by Hellman (1916). It defines the vertical distribution of the mean velocity in the longitudinal direction (x-direction) throughout the entire ABL profile:

$$\frac{\bar{u}}{\bar{u}_{\text{ref}}} = \left(\frac{z-d}{z_{\text{ref}}-d} \right)^{\alpha} = \left(\frac{\tilde{z}}{\tilde{z}_{\text{ref}}} \right)^{\alpha}, \tag{2.8}$$

where $\bar{u}(z)$ is the mean velocity at height z above the surface, z_{ref} is the reference height above the surface, d is the displacement height and α is the exponent of the power law, which is a function of the aerodynamic surface roughness z_0. This model is valid above the displacement height d, i.e. above the objects on the ground. According to ESDU 72026 [8], the displacement height is equal to the height of the buildings on the ground ($d = h$).

2.2.2.4. Logarithmic law

The model that accurately represents the lower 10% of the ABL thickness was originally proposed by Thuillier and Lappe (1964). Also called the law of the wall, the logarithmic relation for the mean velocity profile is defined as follows:

$$\bar{u} = u_{\tau} \frac{1}{\kappa} \ln \left(\frac{z-d}{z_0} \right), \tag{2.9}$$

where u_{τ} is the friction velocity and κ is the von Kármán constant obtained based on experiments in wind tunnels and in the atmosphere. The standard value for the von Kármán

constant is κ =0.4. Friction velocity u_τ is commonly obtained using the fitting procedure as described by Gromke and Ruck [9] and Kozmar [10].

Time-averaged velocity profiles in the ABL for different types of terrain with corresponding values for the aerodynamic surface roughness length z_0, boundary layer thickness δ and the exponent of the power law α are presented in Figure 2.12 [11].

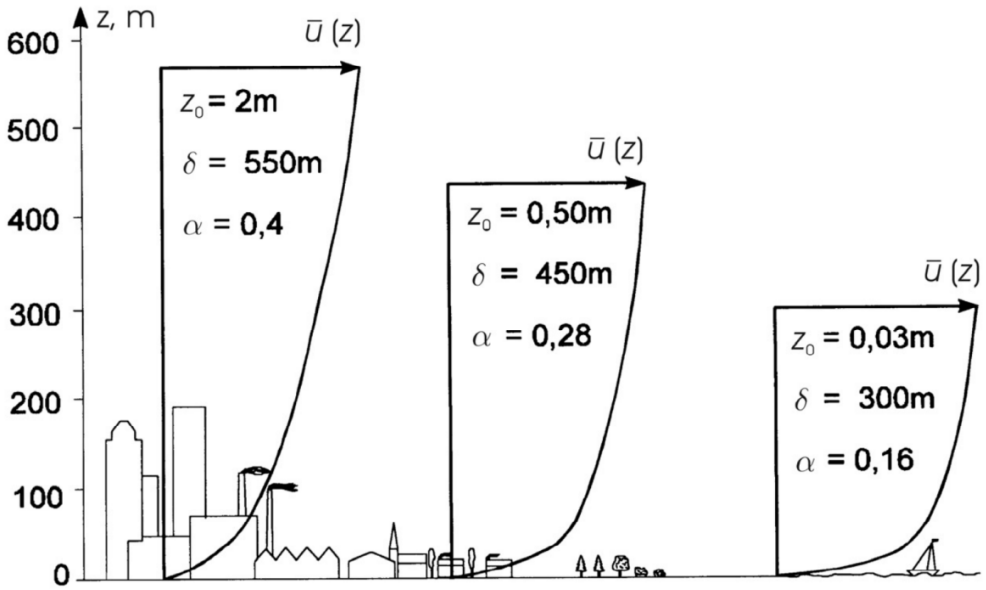

Figure 2.12 Time-averaged velocity profiles in the ABL for different types of terrain, Pernpeintner [11]

2.2.3. Turbulence in the ABL

The ABL is the only part of the atmosphere that is observed in environmental aerodynamics and wind engineering, because most of the engineering structures are located in this layer. Wind turbulence influences structures in several ways, e.g. it causes unsteady loads, wind fluctuations enhance structural vibrations, etc. Therefore, in order to investigate effects of wind turbulence on structures, precise data about ABL turbulence characteristics is very important. The parameters that describe turbulence are turbulence intensity, integral length scale of turbulence, turbulent Reynolds shear stress and power spectral density of velocity fluctuations.

2.2.3.1. Turbulence intensity

Turbulence intensity describes the fluctuating component of the velocity normalized with the value of the mean reference velocity in the main wind direction. Wind velocity fluctuations

occur in all three directions, as ABL turbulence is anisotropic [12]. The longitudinal turbulence intensity is defined as:

$$I_u = \frac{\sqrt{\overline{u'^2(z)}}}{\overline{u}_{\text{ref}}}, \tag{2.10}$$

where $u'(z)$ is the fluctuating component of the velocity in longitudinal direction at height z and $\overline{u}_{\text{ref}}$ is the mean velocity in the longitudinal direction. $\overline{u}_{\text{ref}}$ is commonly measured at the boundary layer thickness height δ, measuring point height z, or at the height of the studied structural model. Similarly, turbulence intensities for the lateral and vertical direction are:

$$I_v = \frac{\sqrt{\overline{v'^2(z)}}}{\overline{u}_{\text{ref}}} \text{ and } I_w = \frac{\sqrt{\overline{w'^2(z)}}}{\overline{u}_{\text{ref}}}. \tag{2.11}$$

The value of the turbulence intensity is the largest in the longitudinal direction and smallest in the vertical direction. According to Counihan [6], the relations between turbulent intensities are constant near the surface:

$$I_u : I_v : I_w = 1 : 0.75 : 0.5. \tag{2.12}$$

Previous studies indicate that turbulence intensity decreases with increasing terrain (surface) roughness and increasing height.

2.2.3.2. Integral turbulent length scale

Integral turbulent length scales are the measures of the vortices in the flow, i.e. the average sizes of wind gusts. They depend on height z above the ground and on terrain roughness. There are in total nine integral turbulent length scales:

$L_u^x,\ L_u^y,\ L_u^z$ for turbulence component u in x-direction (longitudinal)

$L_v^x,\ L_v^y,\ L_v^z$ for turbulence component v in y-direction (lateral)

$L_w^x,\ L_w^y,\ L_w^z$ for turbulence component w in z-direction (vertical)

The most important integral length scale is L_u^x that defines size of eddies in the longitudinal direction due to the velocity pulsations in the longitudinal direction:

$$L_u^x = \int_0^\infty R_u^x(\Delta x)\,\mathrm{d}\Delta x. \tag{2.13}$$

It is commonly calculated using the correlation coefficient R_u^x and assuming Taylor's frozen turbulence hypothesis, which indicates that velocity fluctuations are moving with the mean flow velocity. The correlation coefficient R_u^x:

$$R_u^x(\Delta x) = \frac{\overline{u_1'(t) \cdot u_1'(t-\Delta t)}}{\overline{u_1'^2}} = R_u^x(\Delta t);\ \Delta t = \frac{\Delta x}{2}. \tag{2.14}$$

In addition, turbulent length scales can be calculated as suggested in ESDU 82026 [7] as well:

$$L_u^x = \frac{0.146 \cdot \overline{u}_z}{f_m}, \tag{2.15}$$

where $\overline{u}_z$ is the mean flow velocity in the longitudinal direction at height z and f_m is the peak frequency in the velocity power spectra.

2.2.3.3. Power spectral density of longitudinal velocity fluctuations

Velocity power spectra describe the frequency content of wind-speed fluctuations. Lower frequencies indicate larger-scale motion or larger-scale eddies, while higher frequencies indicate small-scale motions. In practical use, the spectra of turbulent kinetic energy in the longitudinal direction is observed:

$$\overline{u_1'^2} = \int_0^\infty S_u(f)\,\mathrm{d}f, \tag{2.16}$$

where $S_u(f)$ is the amplitude of longitudinal velocity fluctuations at frequency f.

A typical distribution of turbulent kinetic energy is presented in Figure 2.13 [12], with two distinctive areas, i.e. the macrometeorological caused by atmospheric pressure fields, and the micrometeorological due to local changes in terrain. In environmental aerodynamics and wind engineering, only the micrometeorological area is observed with an emphasis on the area of frequencies near the maximal value of turbulent kinetic energy in the longitudinal direction [12].

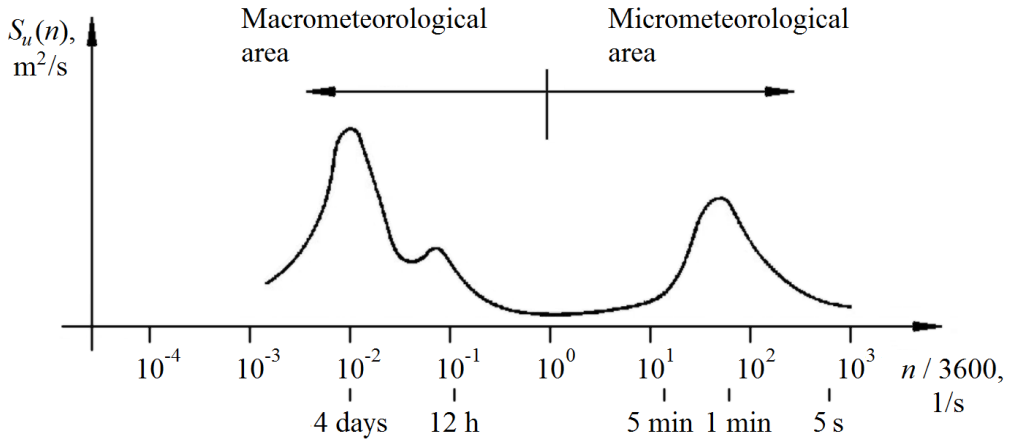

Figure 2.13 Spectrum of turbulent kinetic energy in the longitudinal direction, Kozmar [12]

The eddies that form in a flow over a rough surface dissipate in smaller eddies thus transferring the kinetic energy from larger eddies to smaller ones. This process is called the energy cascade. The Kolmogorov law is valid in the inertial subrange:

$$S_u(f) \approx k_w^{-2/3}, \tag{2.17}$$

where k_w is the wave number of the eddies. Counihan [6] indicates that the eddy size can belong to three different categories that was further elaborated by Kaimal and Finnigan [2], Figure 2.14 [13]:

a) The energy-containing range: A low frequency range which contains the bulk of the turbulent energy and where energy is produced by buoyancy and shear;

b) The inertial subrange: An intermediate range which follows the Kolmogorov law, where energy is neither produced nor dissipated but handed down to smaller eddies;

c) The dissipation range: A high frequency range, where viscous forces dominate and where kinetic energy is converted into internal energy (heat).

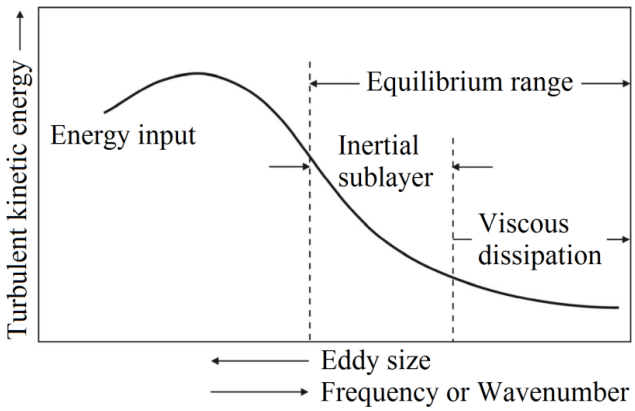

Figure 2.14 Schematic view of the wind velocity power spectrum, Garratt [13]

Pröpper [14] compared theoretical and experimental results and suggests that the Kolmogorov energy distribution term represents a good match with the results in the atmosphere:

$$\frac{f \cdot S_u(f)}{\overline{u'}} = \frac{4 \cdot X_u}{\left(1 + 70,78 \cdot X_u^{\,2}\right)^{5/6}}, \tag{2.18}$$

where X_u is the nondimensional frequency:

$$X_u = \frac{f \cdot L_u^x(z)}{\overline{u}(z)}. \tag{2.19}$$

2.2.3.4. Turbulent Reynolds shear stress

The dominant component of the Reynolds shear stress $-\rho\overline{u'w'}$ represents a measure for vertical transport of longitudinal velocity fluctuations:

$$\tau = \mu\frac{\partial\overline{u}}{\partial z} - \rho\overline{u'w'}, \tag{2.20}$$

where $\mu(\partial\overline{u}/\partial z)$ represents the viscous term or the viscous stress while $\rho\overline{u'w'}$ represents the turbulent Reynolds shear stress or just Reynolds stress. The Reynolds shear stress is maximal close to the surface and it decreases with increasing height. While there are three different components of the Reynolds shear stress, i.e. $\overline{u'v'}$, $\overline{v'w'}$ and $\overline{u'w'}$, only the $\overline{u'v'}$ component is commonly considered, as two remaining components are commonly neglected.

2.3. Wind-tunnel simulation of the ABL

There are several methods for generating a model of the atmospheric boundary layer in a wind tunnel. The differences between the methods are basically the length of the test section and the choice of objects for generating the flow structure. The objects for generating the flow structure are needed because the air flow at the entrance of the wind-tunnel test section is uniform with very low turbulence intensity which is not a valid representation of flow and turbulence characteristics in the atmosphere.

Since every ABL simulation in a wind tunnel is supposed to be a reliable model of the ABL in full scale, it is necessary to determine the simulation length scale factor. This length scale factor is determined using the z_0 aerodynamic surface roughness length and the L_u^x turbulent length scale measured in the wind tunnel, as suggested in Cook [15].

2.3.1. Boundary layer wind tunnels with long test section

The ABL in the atmosphere develops as the flow streams over obstacles (mountains, buildings, etc.) on the Earth surface. The same is achieved in boundary layer wind tunnels with long test section, when the air flows above surface roughness elements only, i.e. without additional experimental hardware. This method creates an ABL simulation that matches well the prototype ABL with respect to the averaged and turbulent structure.

Cermak [16] proposed that a long test section wind tunnel may be defined as a wind tunnel with sufficient length to produce a naturally developed ABL simulation with a nominal thickness in the range between 0.5 m and 1 m at a free stream flow velocity of approximately 10 m/s. Usual simulation length scales for long test section wind tunnels are from 1:500 to 1:1000 [5]. However, when using this method the ABL simulation requires approximately 20 m long test section to reach the ABL simulation thickness of approximately 400 mm. This means that the ABL simulation thickness δ increases very slowly. Simultaneously, along with the generation of the ABL simulation at the bottom surface of the test section, other adverse boundary layers are created on the ceiling and the side walls. This leads to a virtual decrease of the cross section of the test section. Therefore boundary layer wind tunnels with long test section are rarely used [5].

2.3.2. Boundary layer wind tunnels with short test section

Boundary layer wind tunnels are commonly designed with a short test section, as they prove to be nearly as effective as boundary layer wind tunnels with long test section, while considerably less expensive. The adverse boundary layers that are created on the ceiling and the side walls in a short test section are significantly thinner compared to those in the long test sections, thus allowing for the cross section to be more suitable for model experiments.

In order to generate a ABL simulation with a certain thickness in a short test section wind tunnel, surface roughness elements and other experimental hardware are commonly used. There are several methods for creating an ABL simulation, where each of those methods basically uses three main components, i.e. barrier, surface roughness elements and objects that enhance mixing of the air flows.

Plate [17] gives a an overview of the Counihan, Cook and Teunissen method for ABL simulation in a short test section wind tunnel. In the Counihan method, Figure 2.15 [17], elliptically shaped vortex generators are used for the initial generation of a turbulent structure. A net for intensifying the mixing of air flow is used in the Cook method, Figure 2.16 [17],

while in the Teunissen method, Figure 2.17 [17], air is blown inside the test section through a set of fan blowers. Even though a good mean velocity profile can be created in the wind tunnel using the Teunissen method, it is rarely used as there are difficulties with creating an appropriate turbulent structures.

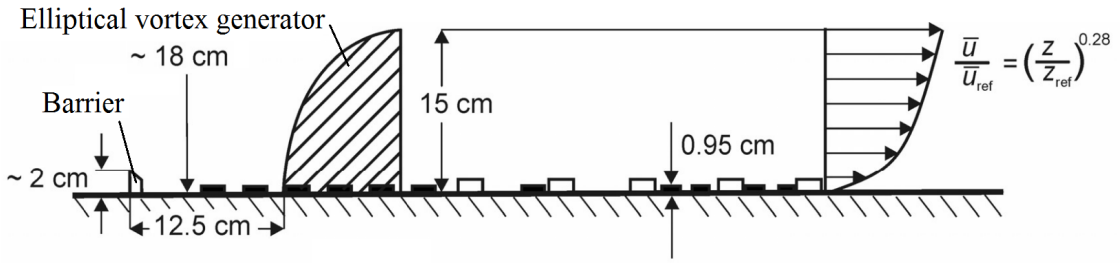

Figure 2.15 The Counihan method for the ABL simulation, Plate [17]

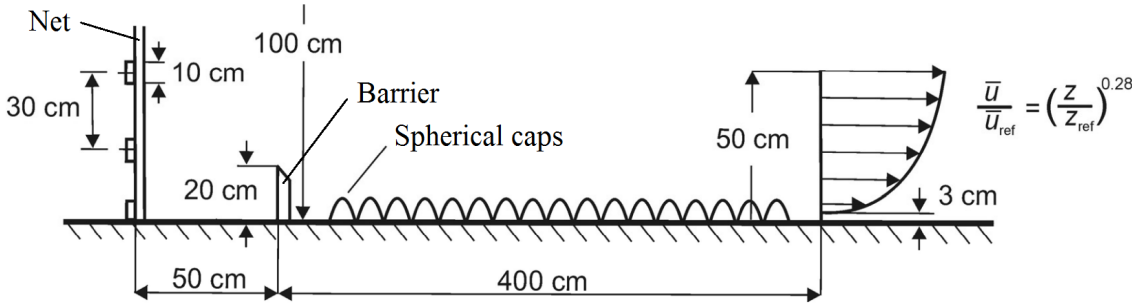

Figure 2.16 The Cook method for the ABL simulation, Plate [17]

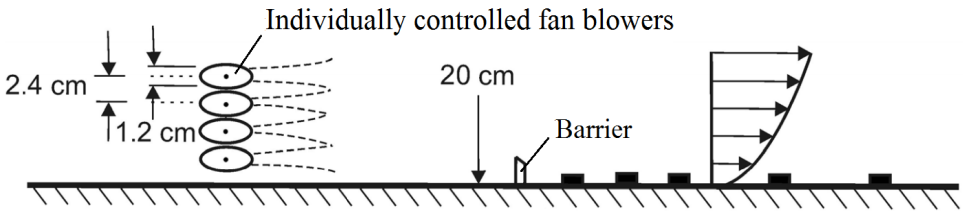

Figure 2.17 The Teunissen method for the ABL simulation, Plate [17]

In each of those methods, the height and spacing density of surface roughness elements predominantly determine the profiles of mean velocity and turbulence. The barrier and the mixing devices allow for shortening the fetch necessary for the ABL simulation fully to develop. The barrier causes a rapid loss of momentum in the lower parts of the ABL simulation and enhances turbulence. Usual simulation length scales in short test section wind tunnels are from 1:100 to 1:1000 [5].

2.3.3. Counihan method for ABL simulation

The basic principle of creating an ABL simulation using the Counihan method is reported in Figure 2.18 [10].

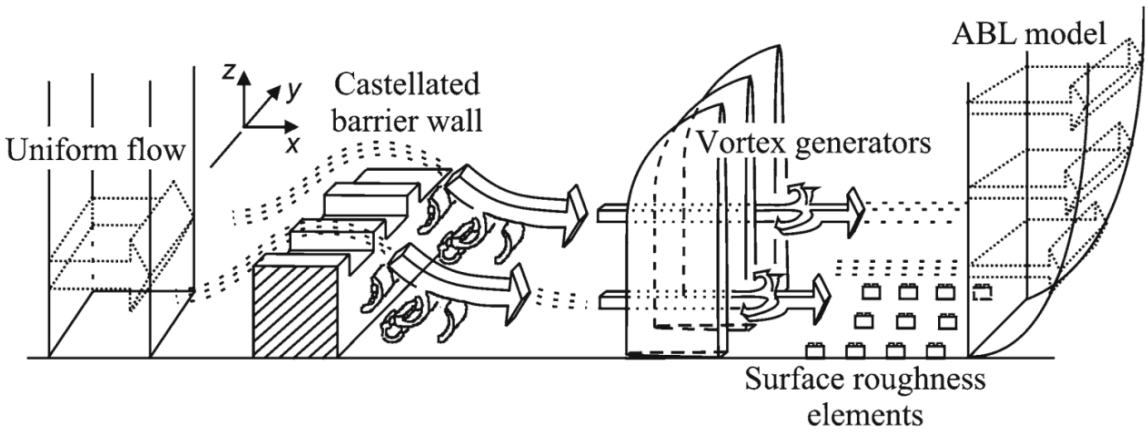

Figure 2.18 Basic principles of the ABL wind-tunnel simulation using the Counihan method, Kozmar [10]

A castellated barrier wall is installed at the inlet of the test section. When air flows over the barrier, eddies with a horizontal axis of rotation are created. Vortex generators are installed downwind of the barrier. They generate eddies with a vertical axis of rotation. While the air passes over the surface roughness elements, the ABL simulation is created. At a distance of approximately three to four ABL simulation thicknesses downwind of vortex generators, the ABL is developed and uniform [6].

2.3.4. Full-depth and part-depth ABL simulations

According to Counihan [6] and other relevant studies, the ABL simulation thickness δ_m is approximately equal to the height of vortex generators. If the vortex generators are truncated, i.e. shortened, Figure 2.19 [18], it is possible to simulate only the lower portion of the ABL.

The advantage of the part-depth ABL simulation using the truncated Counihan vortex generators is in a better resolution of flow and turbulence characteristics and their effects on structures near the ground [18].

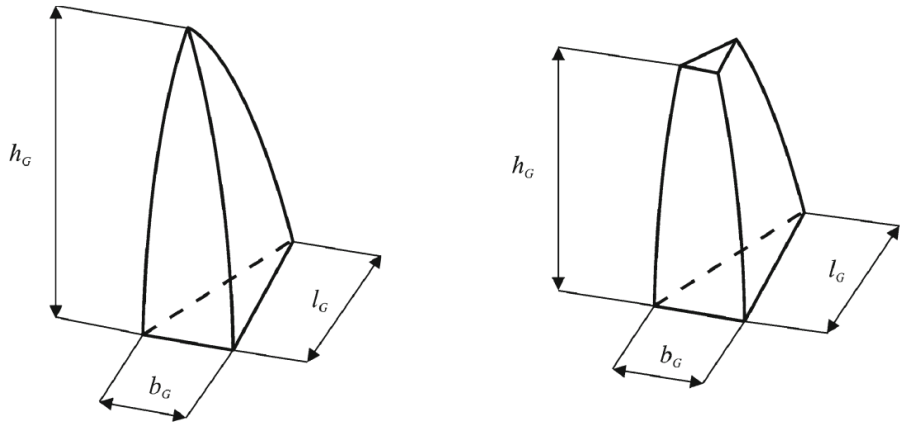

Figure 2.19 Design of classical and truncated Counihan vortex generators, Kozmar [18]

Figure 2.20 shows the basic principles of full-depth and part-depth ABL wind-tunnel simulations.

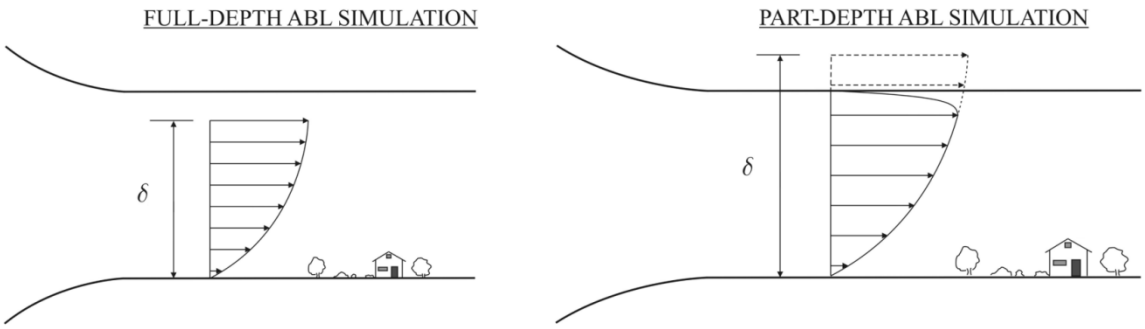

Figure 2.20 Basic principles of full-depth and part-depth ABL wind-tunnel simulations, Kozmar [19]

Full-depth simulation are commonly used in studies on wind loading of tall structures and dispersion of air pollutants, whereas part-depth simulations are used for studies involving low-rise structures [19]. In this thesis, a full-depth ABL simulation was created.

3. WIND-TUNNEL EXPERIMENTS

3.1. Climatic wind tunnel

The wind-tunnel experiments were carried out in the Climatic Wind Engineering Laboratory of the Centre of Excellence Telč (CET), Czech Republic. The climatic wind tunnel (CWT) is a Göttingen closed-circuit type of a tunnel designed to simulate aeroelastic and aerodynamic effects on structures. In addition to this aerodynamic section, there is also a climatic section, where it is possible to simulate other weather effects, e.g. cold, heat, rain, snow. The following measurements can be carried out in the wind tunnel:

- Aerodynamic (force and moment) measurements,
- Aeroelastic (displacement and rotation) measurements,
- Pressure, velocity (three components), temperature measurements,
- Particle Image Velocimetry (PIV),
- Flow visualisation (via smoke, Helium bubbles).

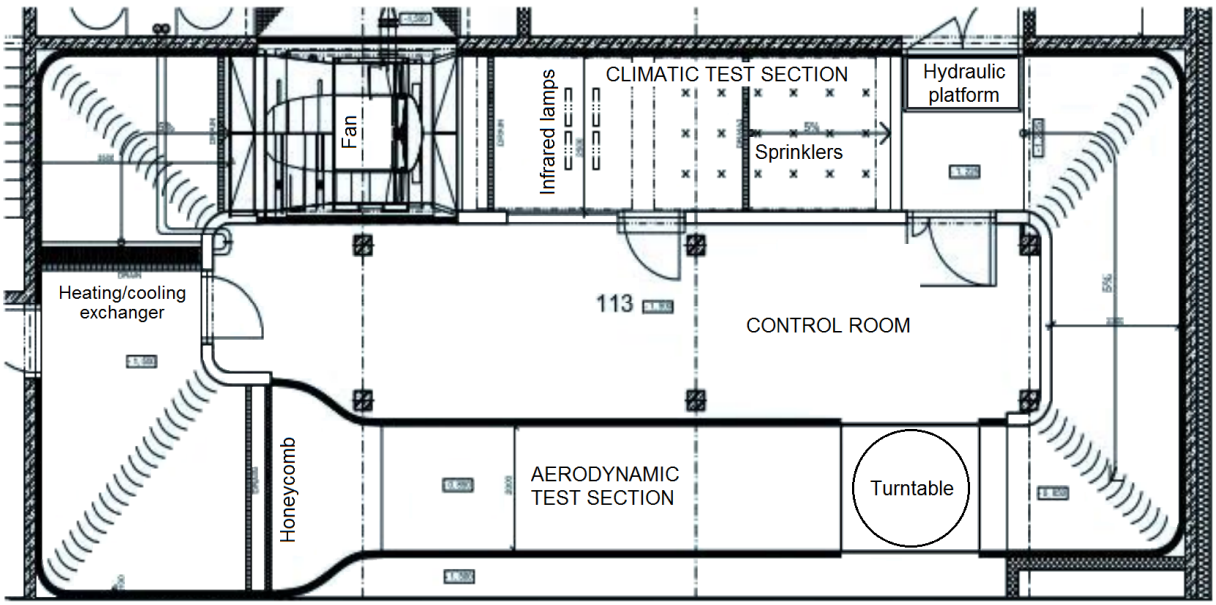

Figure 3.1 Schematic view of the 'Vincenc Strouhal' climatic wind tunnel in the Centre of Excellence Telč

The wind tunnel consists of an inlet section, an aerodynamic section, a climatic section, a return section, a fan section and a heat exchanger. The entire wind tunnel is thermally insulated and every experiment is monitored from the centrally located control room. The schematic view of the wind tunnel is presented in Figure 3.1.

Air flow in the wind tunnel is generated using a large axial fan with a diameter of 2 m. It is equipped with a 200 kW electric motor with adjustable rotation speed via a variable-frequency drive. Temperature conditions inside the wind tunnel can be controlled by means of a 3 m wide and 2.5 m high heat exchanger positioned downwind of the fan. The maximal cooling power is 77 kW resulting in the minimum temperature in the wind tunnel of approximately -10 °C.

3.1.1. Climatic section

Sprinklers are located in the climatic section (Figure 3.2) where precipitation and freezing simulations are performed. The climatic section is designed for research in civil engineering, architecture, heritage care and other fields where thermal effects and precipitation have a significant influence. The climatic section is equipped with infrared lamps for solar radiation simulation.

Figure 3.2 Climatic section with water sprinklers

The cross section is 2.5 m wide and 3.9 m high with a length of 9 m. Depending on the experiment requirements, the height of the climatic section can be adjusted by means of a movable ceiling. The conditions in the climatic section are optimized for the airflow velocity of 15 m/s at 20 °C, while it is also possible to operate at temperatures as low as -5 °C when freezing rain tests are carried out, e.g. Marušić [20].

3.1.2. Aerodynamic section

The aerodynamic section (Figure 3.3) consists of a contraction with a honeycomb followed by the test section with a turntable.

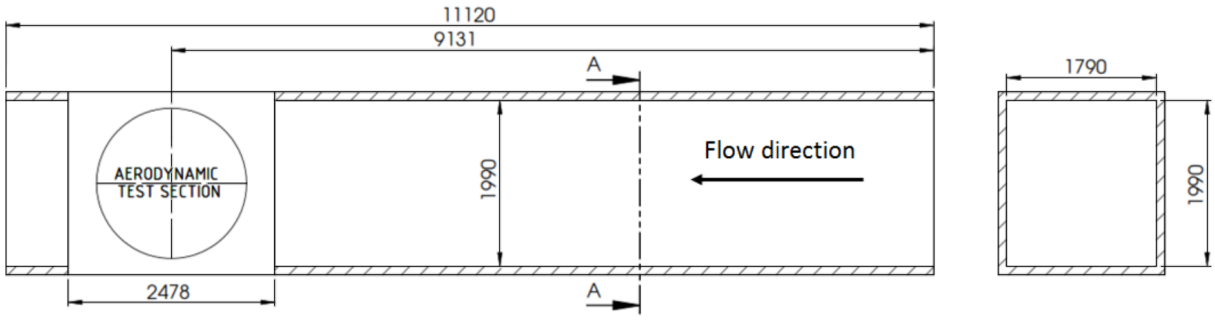

Figure 3.3 Schematic view of the aerodynamic section, dimensions are given in mm

The form of the contraction is determined by a classical potential flow and the ratio is 2.7:1 which allows for the values of turbulence intensity at the test-section inlet to be lower 2% [21]. The 60 mm long honeycomb is placed upwind of the contraction and its basic element is a hexagon with a diagonal of 6 mm. The honeycomb improves flow uniformity and reduces turbulence at the inlet of the test section. In the 11 m long aerodynamic test section there is a turntable that allows for a simulation of wind effect on structures at various wind incidents angles. The turntable center is positioned 9.131 m of the test section inlet. The cross section is 1.9 m wide and 1.8 m high, while the flow velocity can be regulated from 1.2 m/s to 33 m/s.

3.2. Hot-wire anemometry system

The velocity measurements were carried out using hot-wire anemometry. This method relies on the heat transfer between a small heated sensor connected to an electric circuit and the fluid in motion. The sensor of the hot-wire anemometer has a shape of a thin film or a cylindrical wire stretched between two prongs and made of a material with electric resistance

dependent on temperature. There are four types of sensors, i.e. miniature wires, gold-plated wires, fibre-film and film sensors. Depending on a number of sensors there are single-, dual- and triple-sensor probes (Figure 3.4 [22]) also called one-, two- and three-dimensional probes, respectively, where each sensor measures one velocity component.

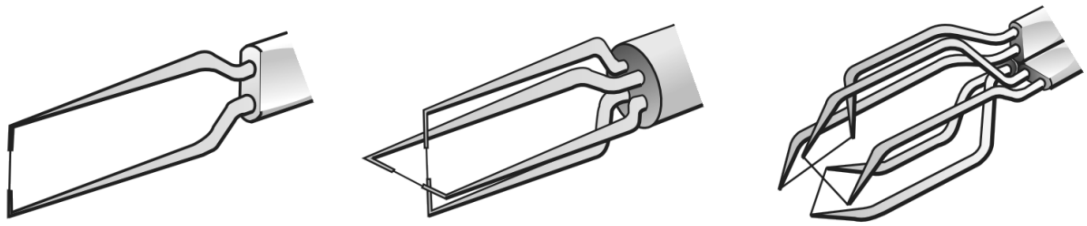

Figure 3.4 One-, two- and three-dimensional hot-wire sensors, Dantec Dynamics [22]

3.2.1. Operating principle and operating modes

Jørgensen [23] described the operating principles of the hot-wire anemometry. Heat is generated in the sensor by the electric current passing through a metal, also called as Joule heating, and it is lost by forced convection. The basic heat balance for a steady flow between heating and cooling is:

$$R_w I_w^{\,2} = \left(T_w - T_a\right)\Phi_{\text{conv}}\left(U\right). \tag{3.1}$$

The left-hand side represents the heating rate where I_w is the current intensity in the sensor and R_w is resistance of the sensor when heated. The right-hand side represents the cooling rate where T_w is the temperature of the wire when heated, T_a is the temperature of the wire at the same location when unheated, and the function $\Phi_{\text{conv}}(U)$ mainly depends on the fluid velocity normal to the wire.

For a turbulent flow, thermal energy is stored in the sensor, and the instantaneous heat balance is:

$$m_w c_w \frac{\mathrm{d}T_w}{\mathrm{d}t} = R_w I_w^{\,2} - \left(T_w - T_a\right)\Phi_{\text{conv}}\left(U\right), \tag{3.2}$$

where m_w is the mass of the sensor and c_w is the specific heat of the sensor material.

A change in velocity causes changes in the electric circuit which can be measured. There are three possible operating modes depending on whether the current, voltage or the resistance (temperature) is constant:

- Constant current anemometry (CCA): The current I_w is constant and the change of velocity U creates a change in resistance R_w which is measured;
- Constant voltage anemometry (CVA): The voltage V_w, which is a product of $R_w I_w$, is constant and change of the current I_w is measured;
- Constant temperature anemometry (CTA): The temperature of the sensor is constant, i.e. R_w is constant, and the change of velocity U creates a change in current I_w which is measured.

3.2.2. Constant temperature anemometry (CTA)

3.2.2.1. Operating principle

The constant temperature anemometry (CTA) was used in this thesis. The main differences between the three operating modes are with respect to the handling of the thermal inertia in the sensor. As explained in Kozmar [5] and Jørgensen [23], the temperature of the sensor in the CTA is maintained constant by a feedback loop and the CTA is designed with the purpose of eliminating the influence of the thermal inertia of the wire in fluctuating flows. Schematic view of the Wheatstone bridge used in the hot-wire sensor is reported in Figure 3.5 [23].

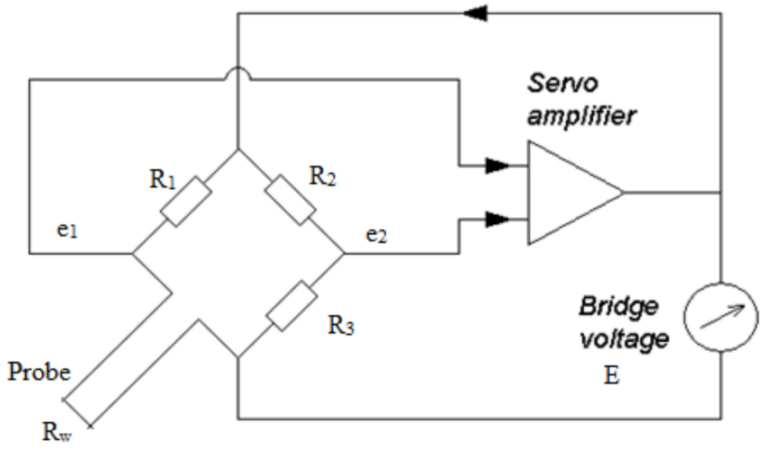

Figure 3.5 Schematic view of the Wheatstone bridge used in the hot-wire sensor, Jørgensen [23]

The hot-wire, with a resistance R_w, is connected to one arm of the Wheatstone bridge and is heated with electric current. The servo amplifier keeps the bridge in balance by controlling the current at the sensor regardless of the cooling imposed by the flow of the fluid. The voltage of the bridge E represents the heat transfer thus being a direct measure of the velocity. Electrical

energy is supplied to the wire at exactly the same rate as heat is lost to the surrounding fluid. This leads to the constant wire temperature regardless of the flow velocity. The frequency limit of the instrument is mainly determined by the electronic circuitry.

3.2.2.2. Experimental technique

The CTA system is a part of a measuring chain, Figure 3.6 [23], consisting of a probe, probe support, probe cable, the CTA anemometer, a signal conditioner, an A/D converter and a computer with the application software.

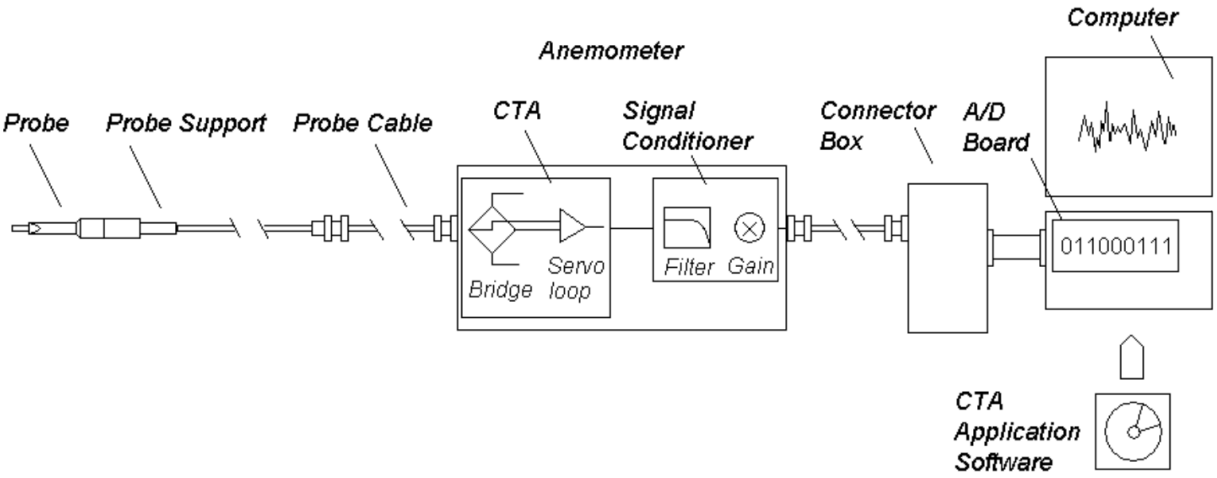

Figure 3.6 CTA measuring chain used in the present study, according to Jørgensen [23]

Dantec Dynamics 55R01 straight general-purpose probes with fibre-film sensors (Figure 3.7 [22]) were used for measurements. The film between the prongs is 70 μm in diameter and 3 mm long, while covered with a 0.5 μm quartz coating for protection against wear and oxidation in gas applications, thus making these probes more robust.

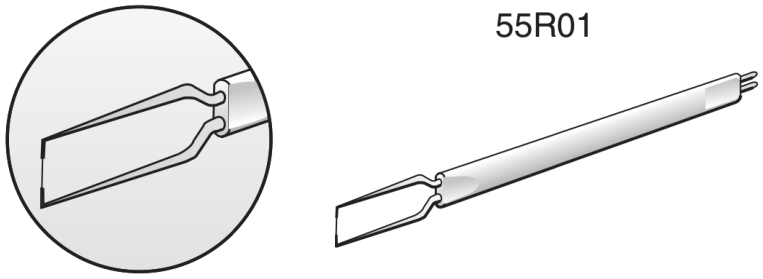

Figure 3.7 Dantec Dynamics 55R01 probes with fibre-film sensors, Dantec Dynamics [22]

The probes were mounted on the Dantec Dynamics 55H21 probe support connected using 20 m long cable to the Multichannel 54N81 CTA System by Dantec Dynamics. The signal conditioner for high-pass and low-pass filtering is a part of the CTA system. The A/D converter allows for analog to digital data conversion, while the data acquisition and analysis are performed on a personal computer using the StreamWare Pro software.

3.2.2.3. Calibration

One hot-wire probe was used for measurements of the ABL simulation while another one was used to measure reference velocity in the free stream. The probes with accompanying cables were calibrated using the automatic Dantec Dynamics StreamLine Pro Calibrator (Figure 3.8). Calibration was performed by Marušić [20] for velocities in range from 0.5 m/s to 40 m/s in 27 points. A fourth-order polynomial was used to fit the calibrated data. Low-pass filter was set at 300 Hz to remove noise.

Figure 3.8 Dantec Dynamics StreamLine Pro Calibrator for hot-wire calibration, Marušić [20]

3.2.3. Traverse system

The modular Dantec Dynamics traverse system is installed in the wind-tunnel test section. Its main purpose is to automate the movement of a measuring device (in this case the CTA probe) between measurement points. It is originally designed and based upon the principles of traverse systems used for Laser Doppler Anemometry (LDA) equipment. The mechanism, made from aluminum, is able to move 660 mm both in lateral and in vertical direction and the movement can be controlled manually or remotely using a computer. The main mechanism is mounted on rails and installed on the ceiling along the entire length of the test section. The mechanism has to be manually positioned in the longitudinal direction. The traverse system with the railings is presented in Figure 3.9.

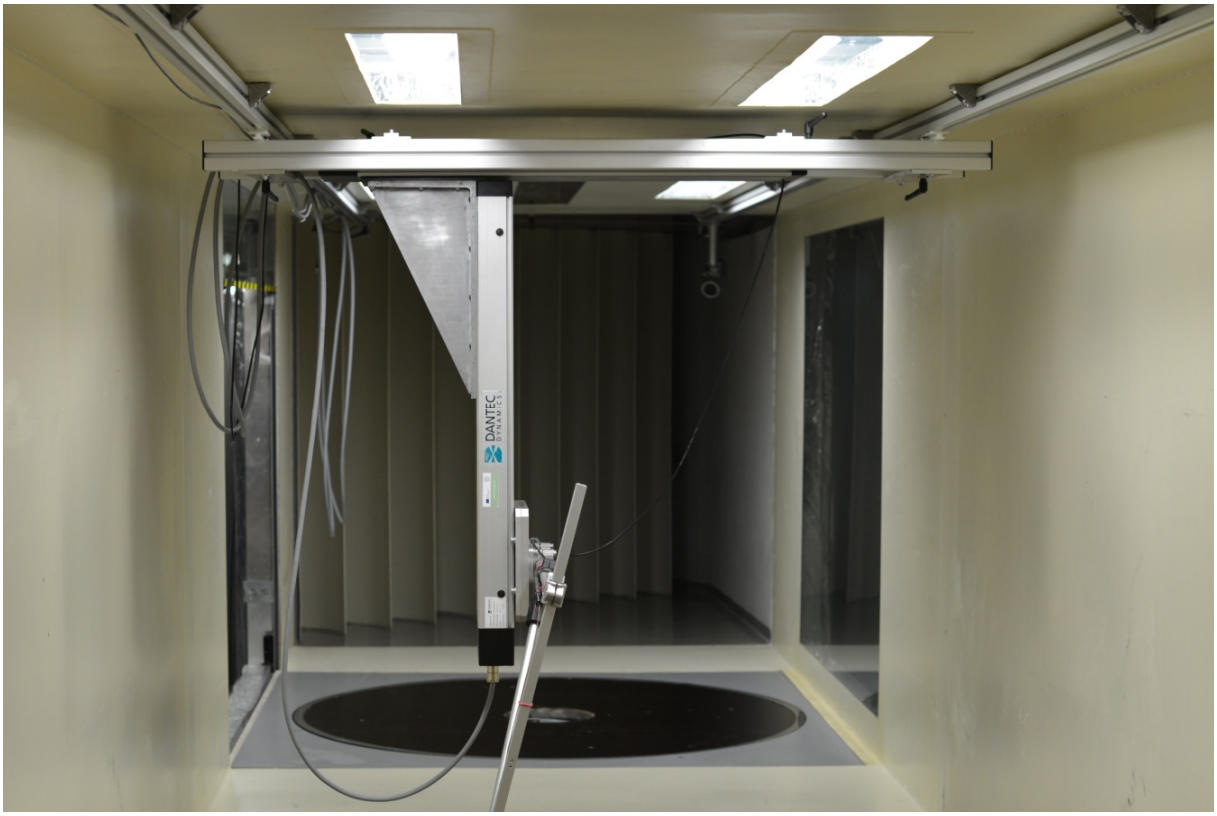

Figure 3.9 Dantec Dynamics traverse system in the aerodynamic test section

3.3. Experimental setup

3.3.1. Counihan method for the ABL wind-tunnel simulation

The Counihan method including the castellated barrier wall, vortex generators and surface roughness elements was used to simulate the ABL in the wind-tunnel test, Figure 3.10 and Figure 3.11.

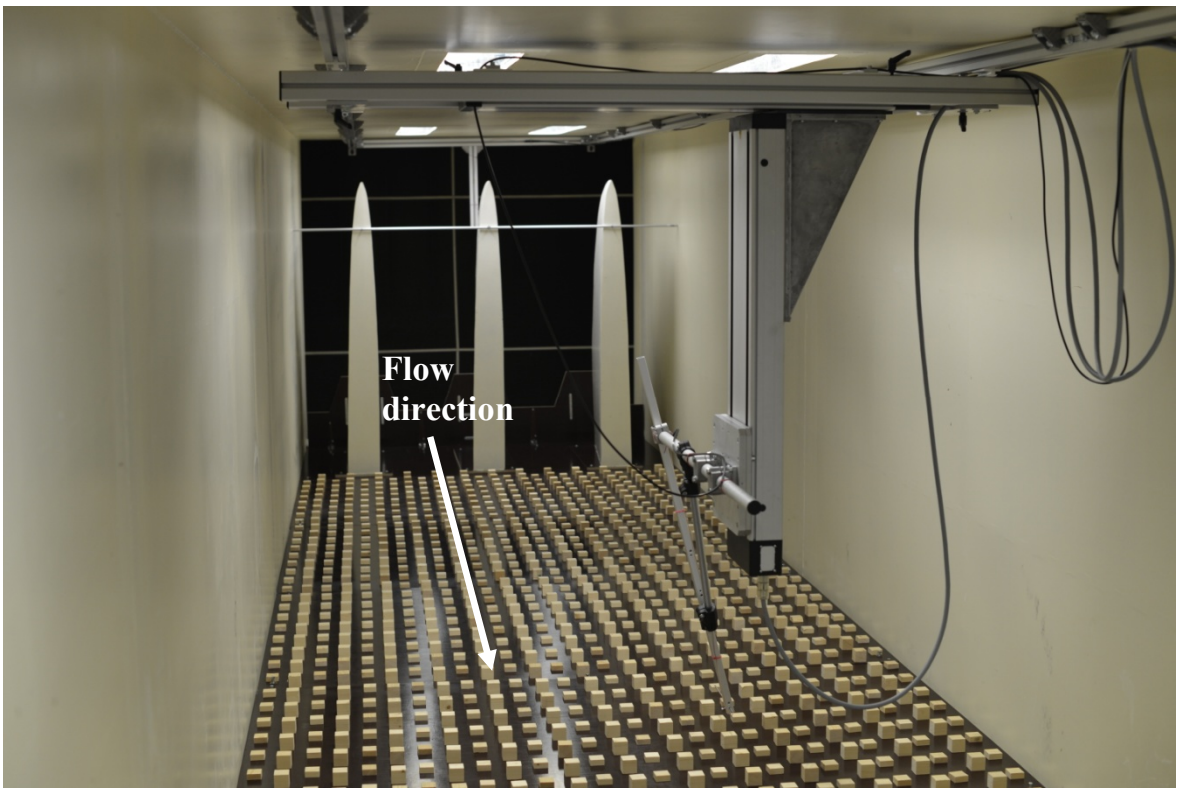

Figure 3.10 Castellated barrier wall, vortex generators and surface roughness elements in the CET climatic wind tunnel

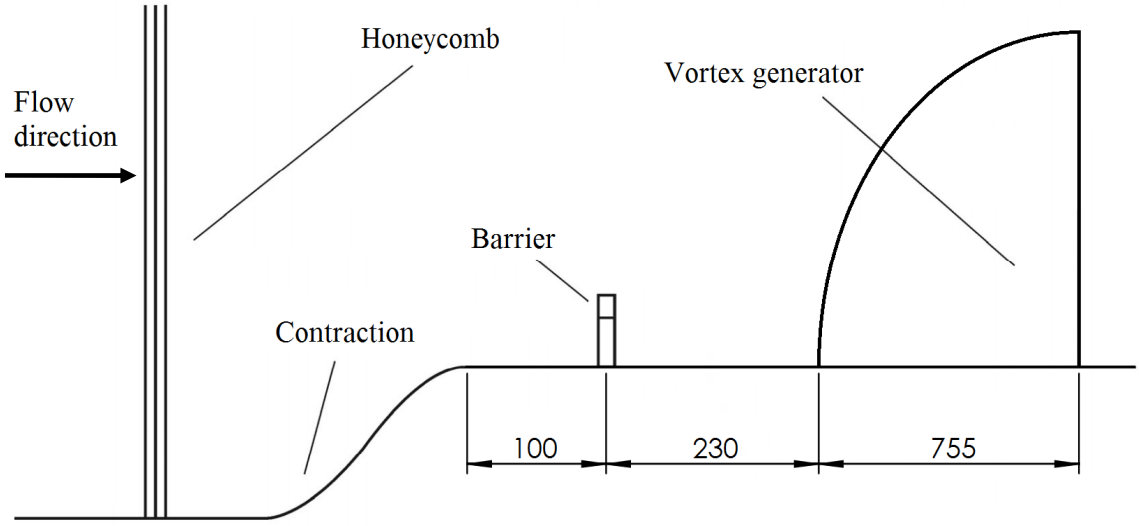

Figure 3.11 Arrangement of the castellated barrier wall and vortex generators in the CET climatic wind tunnel, dimensions are given in mm

Detailed drawings with dimensions of the castellated barrier, vortex generator and surface roughness elements are reported in Figure 3.12, Figure 3.13 and Figure 3.14, respectively.

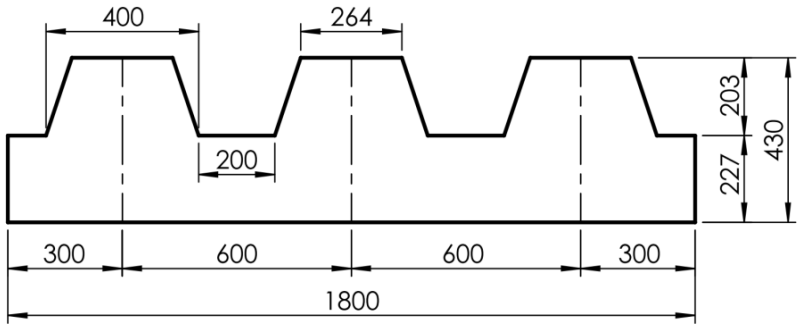

Figure 3.12 Castellated barrier wall, dimensions are given in mm

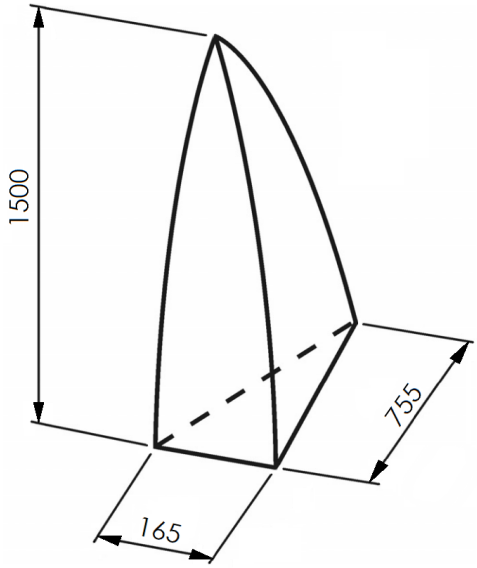

Figure 3.13 Counihan elliptical vortex generator, dimensions are given in mm

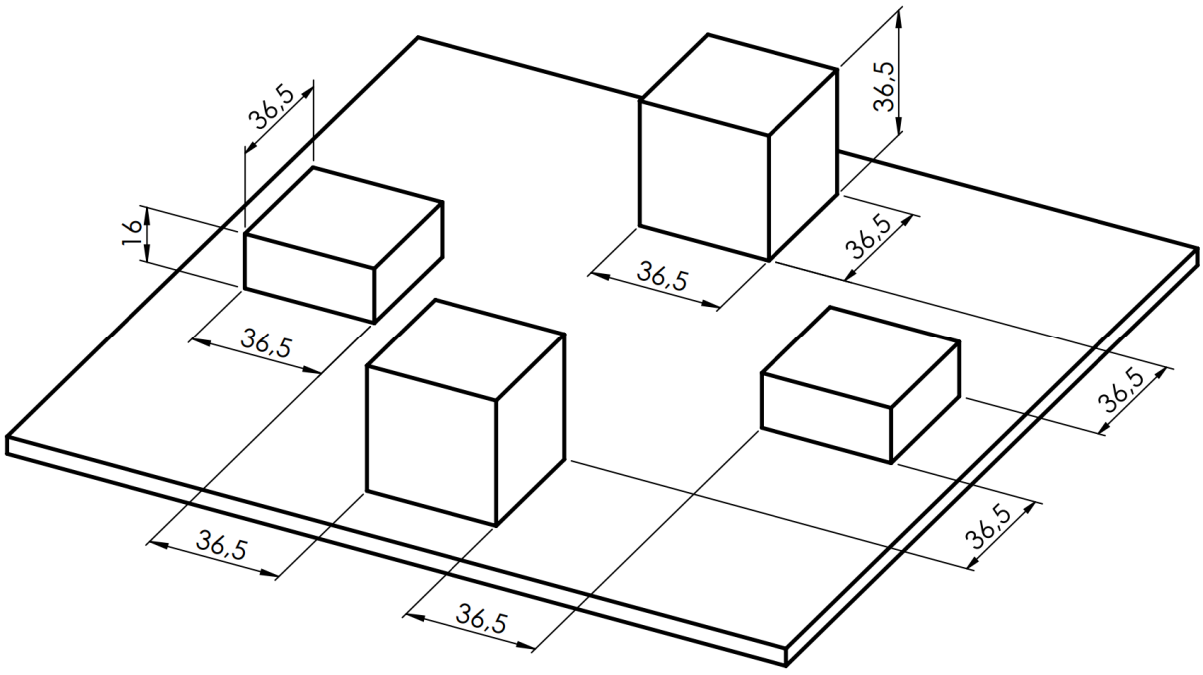

Figure 3.14 Arrangement of surface roughness elements, dimensions are given in mm

3.3.2. Methodology

Velocity and turbulence measurements were carried out in the longitudinal direction using the CTA system. The traverse was manually adjusted in the longitudinal direction, while the movement in the lateral and vertical direction was controlled automatically using the StreamWare Pro software. A hot-wire probe that measured free stream reference velocity was placed at the inlet of the test section above the castellated barrier wall (Figure 3.15).

The development of the lower part of the ABL simulation along the wind-tunnel test section was measured in seven cross sections at various distances downstream of the test-section inlet, Figure 3.15. These positions are indicated as x_1 to x_7.

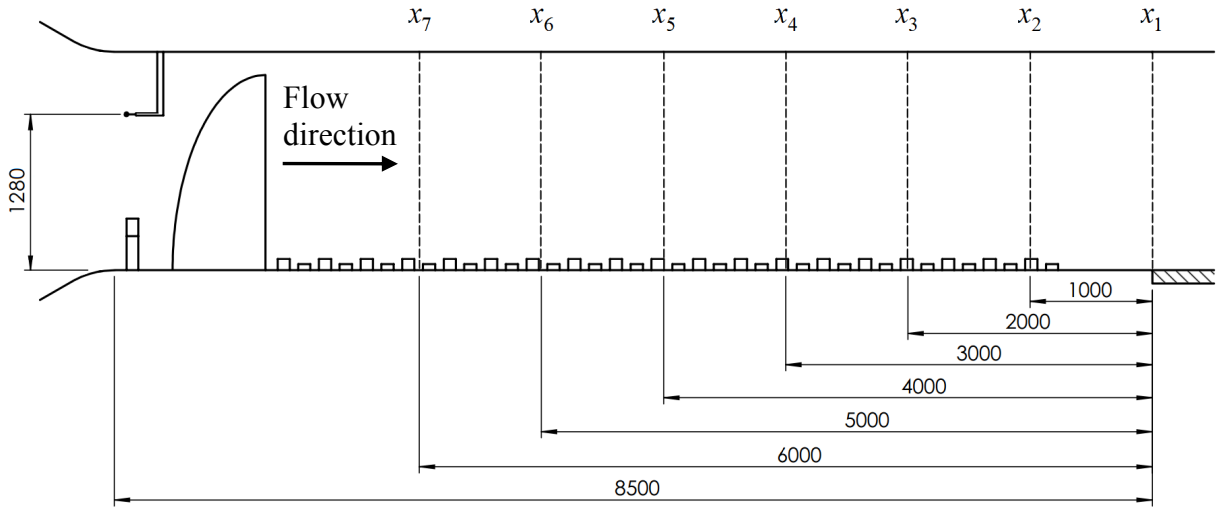

Figure 3.15 Measuring distances in seven cross sections at various distances downstream of the test-section inlet, all measures in mm

In each cross section, measurements were carried out in 21 points along the vertical line. Seven points were examined in the middle (center) of the cross section and seven on both sides, 300 mm to left- and 300 mm to the right-hand side, denoted as y_C, y_L and y_R, respectively (Figure 3.16). So in total, each profile was made out of seven points. The highest point is at 700 mm above the test-section bottom surface.

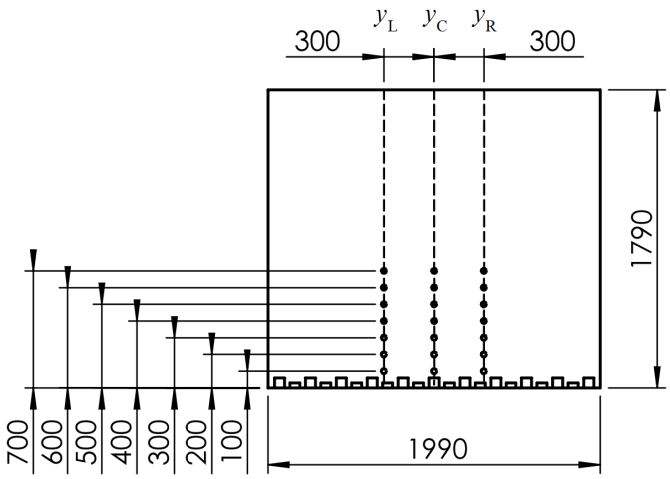

Figure 3.16 Positions of the measuring points in each cross section at seven downstream distances from the test-section inlet, all measures in mm

The total number of measuring points is 147 and each measurement was carried out for five different velocities, i.e. at five different percentages of the maximal fan frequency (10, 20, 30, 35 and 40% of the maximal fan frequency).

The ABL simulations were carried out for several setups of experimental hardware:

- Empty wind tunnel,
- Separately for each element of the Counihan method, i.e. castellated barrier wall, vortex generators and surface roughness elements,
- The ABL simulation using the Counihan method, i.e. combined effects of the castellated barrier wall, vortex generators and surface roughness.

Details of performed experimental configurations are reported in Table 3.1.

Table 3.1 Details of performed experimental configurations

Configuration	Description
# 1	ABL simulation using the Counihan method
# 2	Castellated barrier wall
# 3	Vortex generators
# 4	Surface roughness elements
# 5	Empty wind tunnel

Preliminary measurements were carried out to determine the optimal time record length for these experiments, Table 3.2. The investigated time record lengths were 20 s, 30 s, 60 s, 90 s, 120 s and 180 s, while the sampling frequency of 1000 Hz was used in all tests based on previous experiments [20], [21]. These preliminary measurements were carried out at 40% of the maximal fan frequency, in the lateral center of the test section, in 700 mm height at the leading edge of the turntable.

Table 3.2 Sampling times preliminary test

Sampling time (s)	Mean velocity (m/s)	Relative error (%)
20	13.78	1.12
30	13.78	1.13
60	13.67	0.30
90	13.72	0.63
120	13.62	0.08
180	13.51	0.09
mean:	13.63	

These experimental results indicated a relative error of 1% for the time record length of 20 s. This error was considered to be acceptable and all further experiments were consequently performed for the time record length of 20 s with the sampling rate of 1000 Hz.

4. RESULTS AND DISCUSSION

4.1. Reynolds number effect

The experimental results indicated that the critical roughness Reynolds number Re_R was larger than five in all tested configurations, in agreement with Plate [17]:

$$Re_R = \frac{u_\tau \cdot z_0}{\nu} > 5, \tag{4.1}$$

where ν is the kinematic viscosity of air ($\nu = 1.33 \cdot 10^5$ m^2/s), friction velocity $u_\tau = 0.12$ and aerodynamic surface roughness length $z_0 = 0.9$, thus yielding $Re_R = 26$.

In addition, preliminary experiments were carried out to investigate the Reynolds number sensitivity of the ABL simulation, where mean velocity $\bar{u}$, longitudinal turbulence intensity I_u and the longitudinal turbulent length scales L_u^x were analyzed, Figure 4.1.

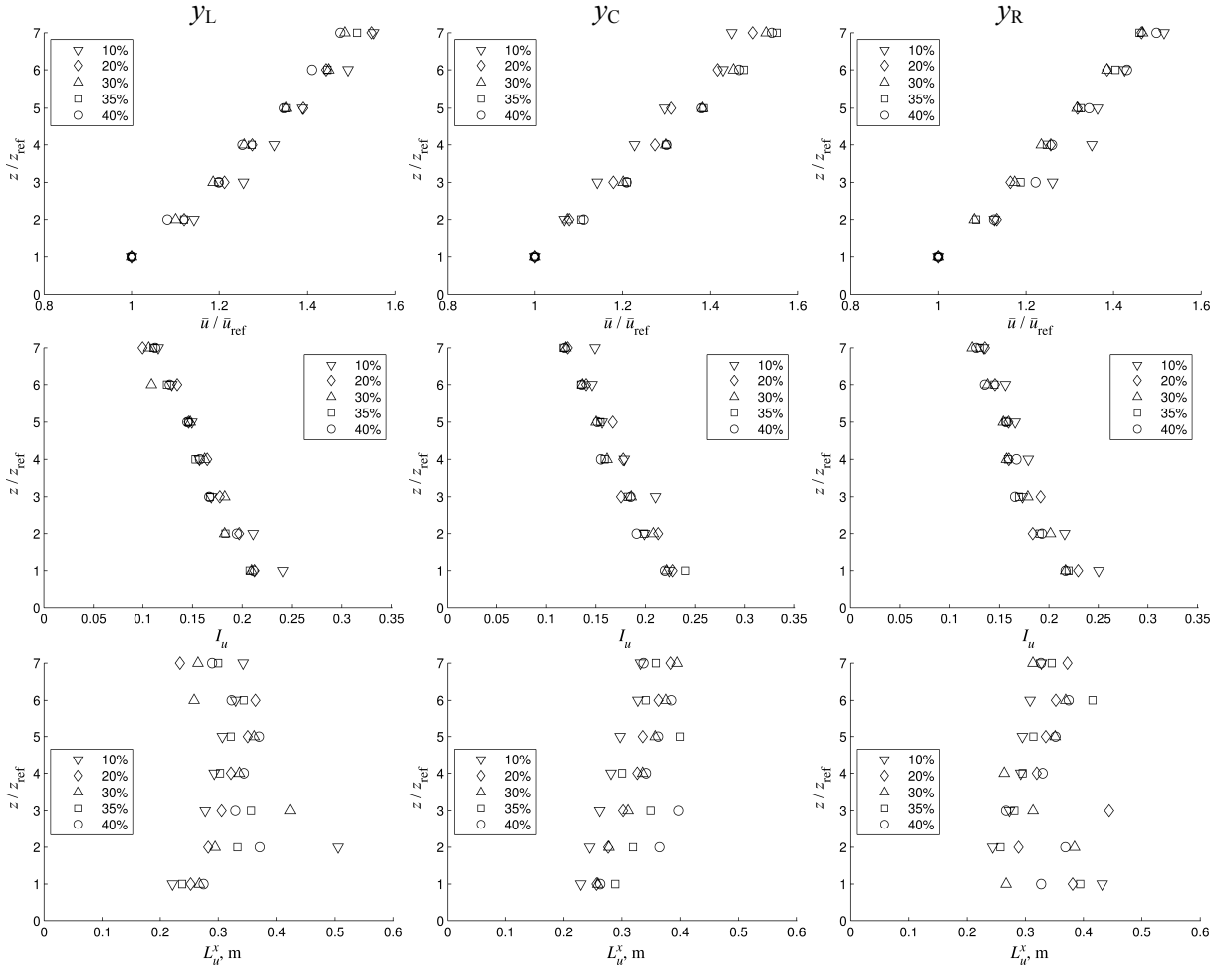

Figure 4.1 Experimental results for the Reynolds number sensitivity of the ABL simulation (z_{ref} = 0.1 m)

For free-stream velocities larger than 13 m/s, the differences in created ABL simulations are negligible. Hence, all further experiments are carried out at velocities larger than 13 m/s, in agreement with previous relevant studies, e.g. Wittwer and Möller [24], where it is recommended to perform the experiments at largest possible velocities.

4.2. Effects of various devices on flow and turbulence characteristics

The effects of the castellated barrier wall, vortex generators and surface roughness elements on flow and turbulence characteristics in the wind-tunnel test section are reported in Figure 4.2, Figure 4.3 and Figure 4.4, where the influence of each of those hardware elements was analyzed separately.

4.2.1. Vertical profiles of the longitudinal mean flow velocity

The mean velocity profiles in #3, #4 and #5 are uniform along the height and constant along the test section. Close to the ground surface a small influence of surface roughness can be observed in #4. On the other hand, in #1 and #2 there is a velocity increase with increasing height from the test-section bottom surface, while the effects of the castellated barrier wall and vortex generators are dying-out when moving further downstream from the test-section inlet.

4.2.2. Vertical profiles of the longitudinal turbulence intensity

Turbulence intensity decreases with increasing height in #1 and #2. A small influence of surface roughness close to the ground surface can be observed in #4. When moving further downstream from the test-section inlet, the effects of the castellated barrier wall and vortex generators are dying-out, which can be observed in #1, #2 and #3. While the effects of vortex generators in their immediate wake are clearly observed their influence ont turbulent intensity profiles decreases when moving downstream through the test section, as at the turntable the values in the turbulence intensity profile in #3 are constant along the height.

4.2.3. Vertical profiles of the integral longitudinal turbulent length scales

Turbulent length scales increase along the length of the test section in #1 and #2. The turbulent length scale profiles are uniform along the height and constant along the test section in #3, #4 and #5. A small influence of surface roughness close to the ground surface can be observed in #4.

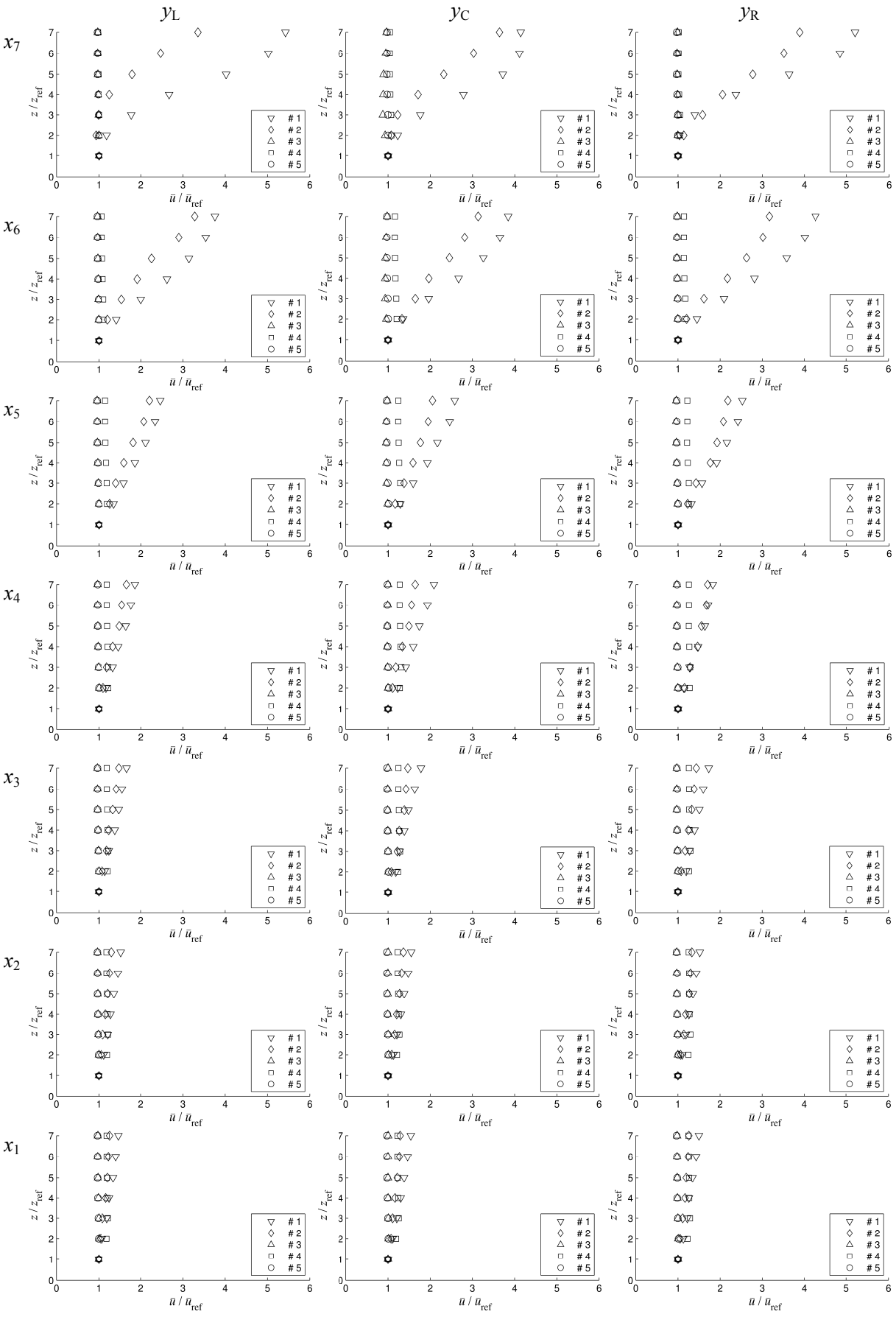

Figure 4.2 Effects of various devices on vertical profiles of mean flow velocity

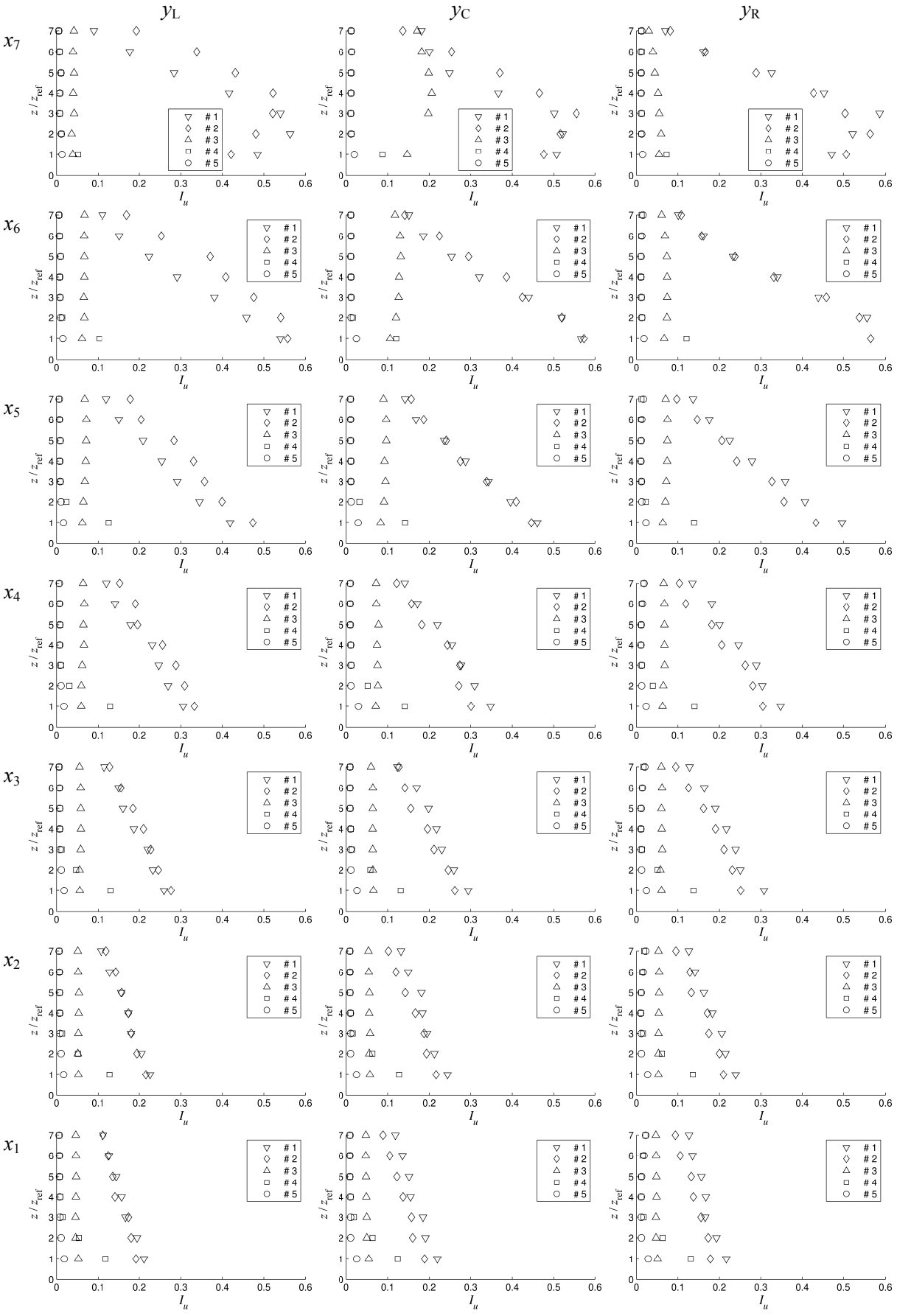

Figure 4.3 Effects of various devices on vertical profiles of turbulence intensity profiles

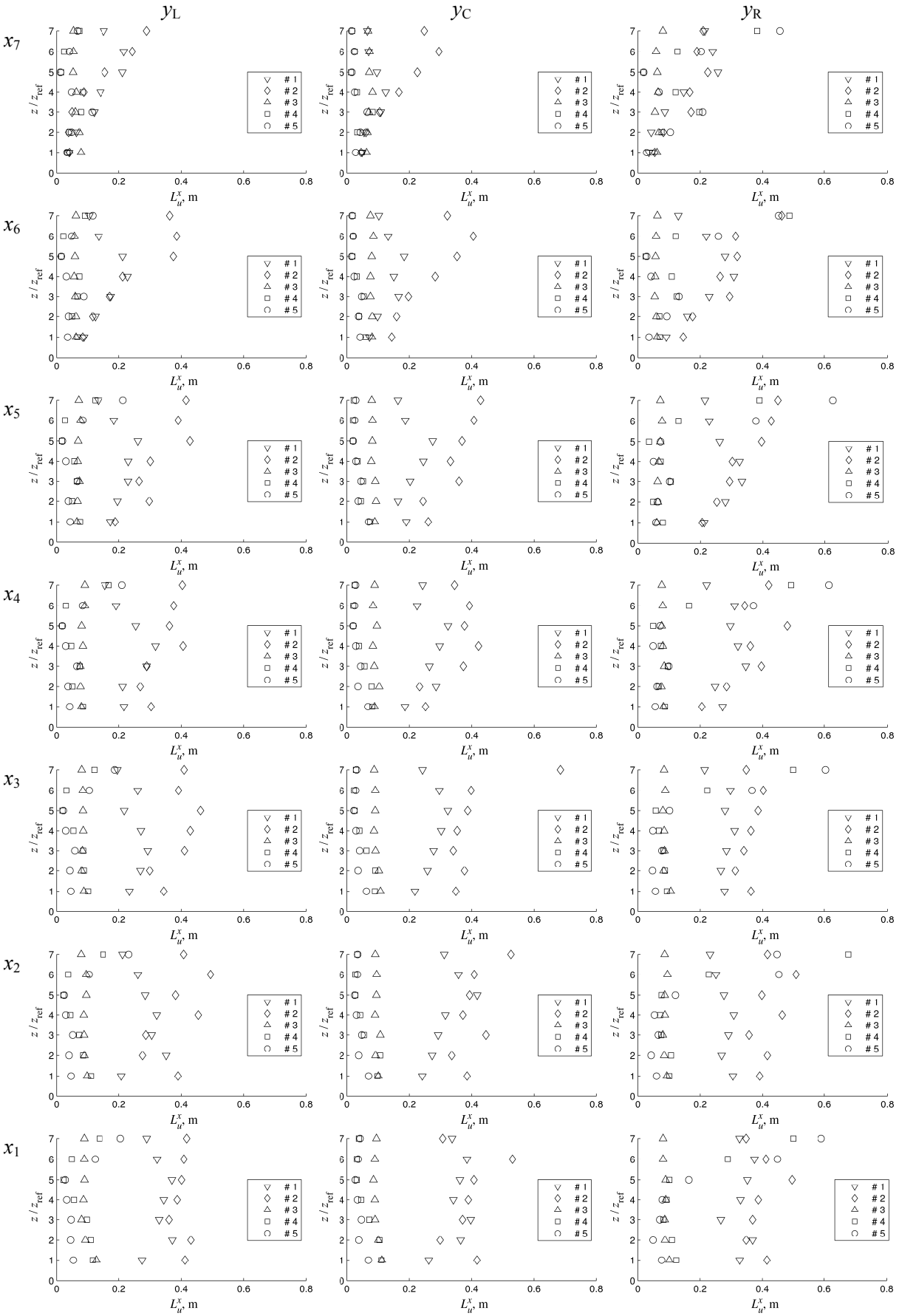

Figure 4.4 Effects of various devices on vertical profiles of turbulent length scales

4.3. Development of the ABL simulation using the Counihan method

The experimental results for the ABL simulation are reported in Figure 4.5, Figure 4.6 and Figure 4.7.

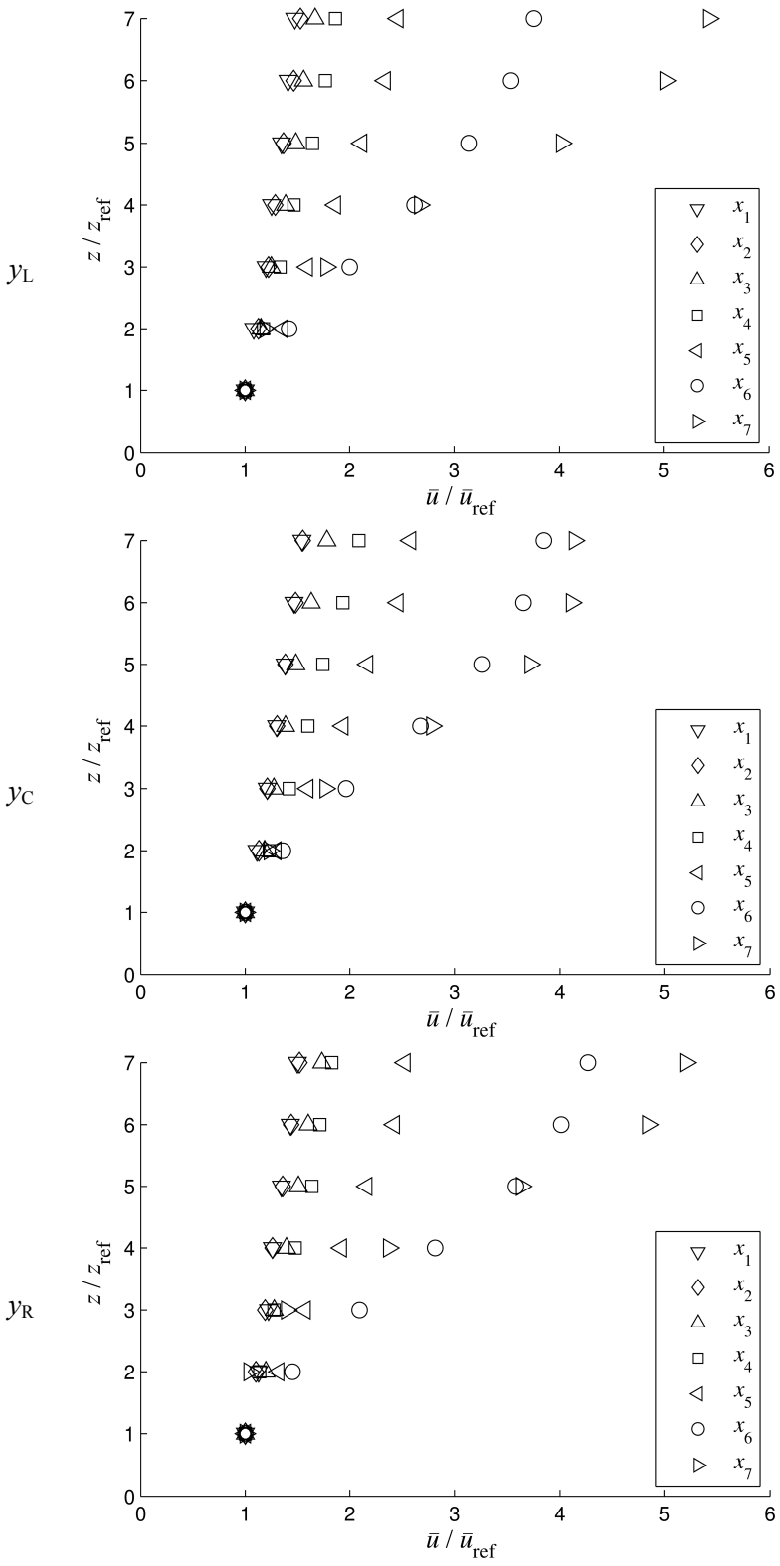

Figure 4.5 Development of ABL mean velocity profiles along the test section

With increasing distance downstream from the vortex generators, the differences in profiles of mean velocity, turbulence intensity and turbulent length scales decrease. Those differences are minimal at the turntable indicating the ABL simulation at this position is fully developed.

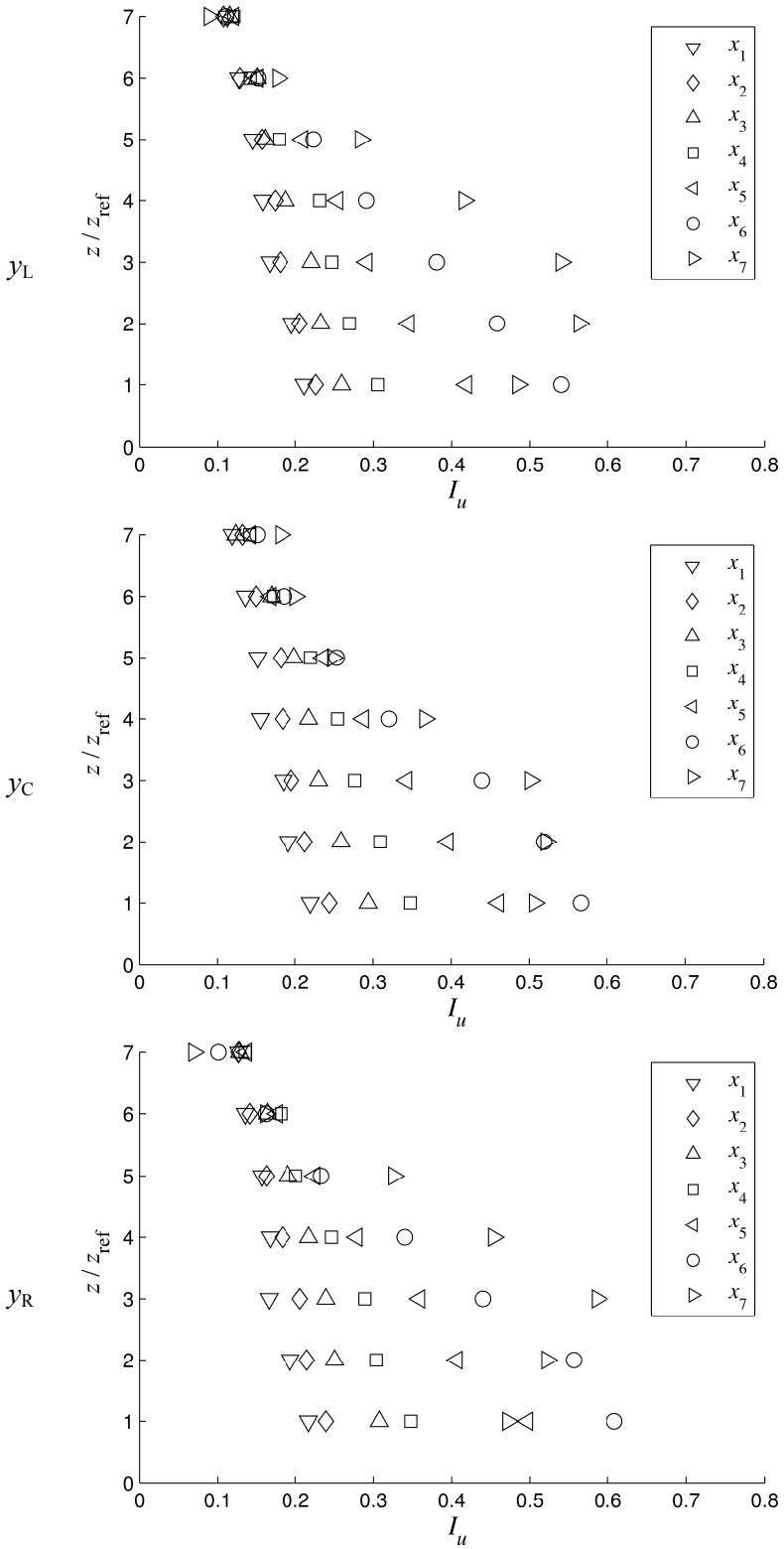

Figure 4.6 Development of ABL turbulence intensity profiles along the test section

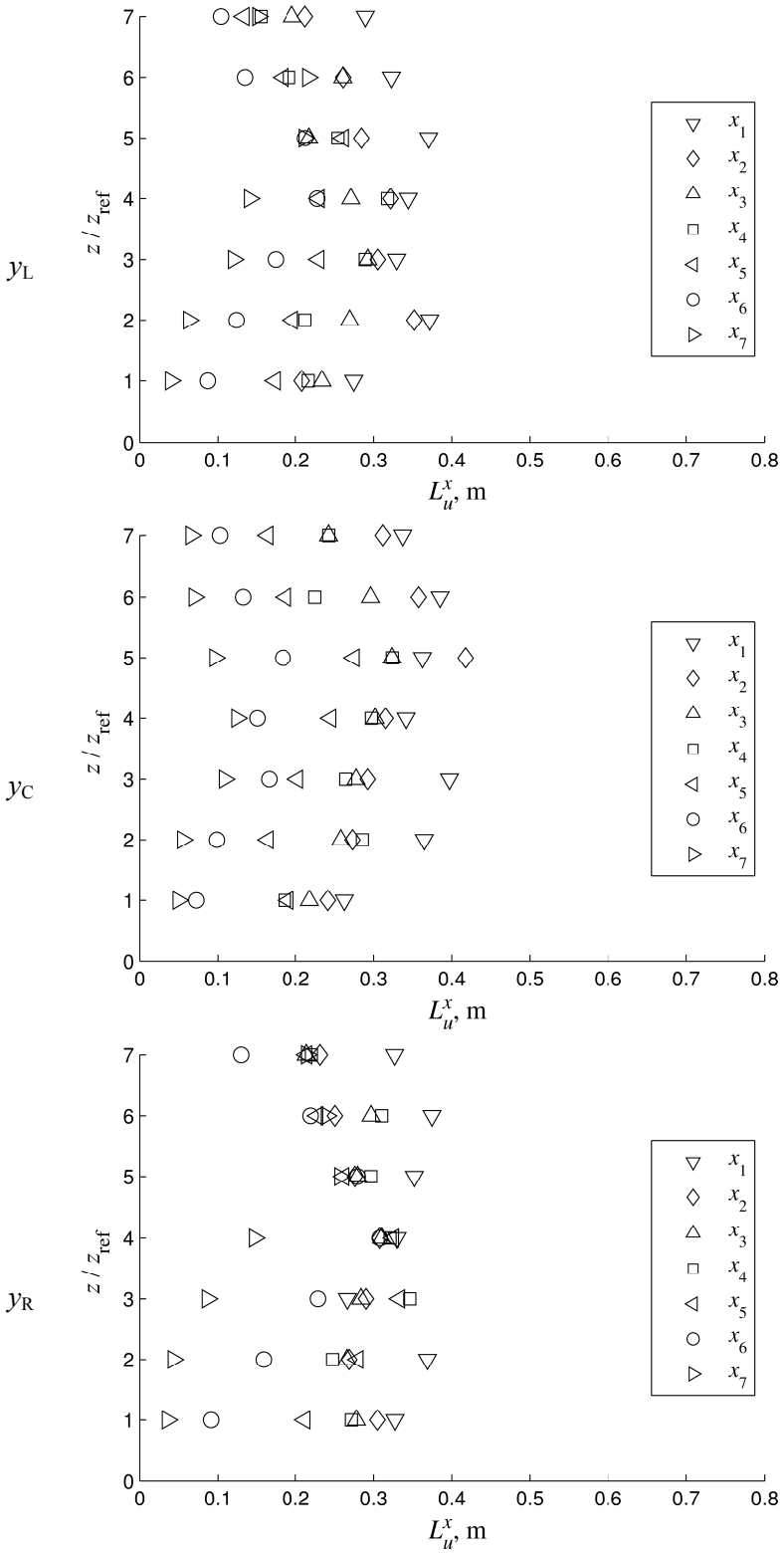

Figure 4.7 Development of ABL turbulent length scales along the test section

4.4. Development and uniformity of the ABL simulation

The statistics for development and uniformity of the ABL simulation is reported in Table 4.1 and Table 4.2, respectively. The flow development was analyzed for the two most downstream positions, i.e. x_1 and x_2, while the flow uniformity in the lateral direction (across the test section) was analyzed at the x_1 position for three measured profiles.

Table 4.1 Longitudinal uniformity of the ABL

$\frac{\overline{z}}{\overline{z}_{ref}}$	$\frac{\overline{u}}{\overline{u}_{ref}}$ (x_1)	$\frac{\overline{u}}{\overline{u}_{ref}}$ (x_2)	Relative difference (%)
1	1.00	1.00	0.00
2	1.11	1.13	1.80
3	1.21	1.21	0.11
4	1.30	1.31	0.38
5	1.38	1.38	0.23
6	1.47	1.48	0.99
7	1.54	1.55	0.58
Mean difference:			0.58

Table 4.2 Lateral uniformity of the ABL

$\frac{\overline{z}}{\overline{z}_{ref}}$	$\left(\frac{\overline{u}}{\overline{u}_{ref}}\right)_{y_L}$	Relative difference (%)	$\left(\frac{\overline{u}}{\overline{u}_{ref}}\right)_{y_0}$	Relative difference (%)	$\left(\frac{\overline{u}}{\overline{u}_{ref}}\right)_{y_R}$
1	1.00	0.00	1.00	0.00	1.00
2	1.08	2.62	1.11	1.42	1.13
3	1.20	0.85	1.21	1.03	1.22
4	1.25	3.64	1.30	3.12	1.26
5	1.35	2.33	1.38	2.58	1.34
6	1.41	3.77	1.47	2.39	1.43
7	1.48	4.27	1.54	2.79	1.50
Mean difference:		2.50		1.90	
Grand mean difference:			2.20		

A mean difference of 0.58% for development of the ABL simulation, and a grand mean difference for the ABL lateral uniformity of 2.20% indicate the ABL simulation at the turntable is fully developed and uniform.

4.5. Comparison of created ABL simulation with international codes and standards

4.5.1. Mean velocity profile

Experimental results for the mean velocity were first fitted to the power law to determine the power-law exponent α using the least-squares method. A logarithmic-logarithmic representation was then used, where the horizontal axis was velocity and the vertical axis was height above the surface. The slope of the straight line created through the measuring points represents the power-law exponent α. Figure 4.8 presents a good agreement of the experimental results in comparison with the power law for $\alpha = 0.20$.

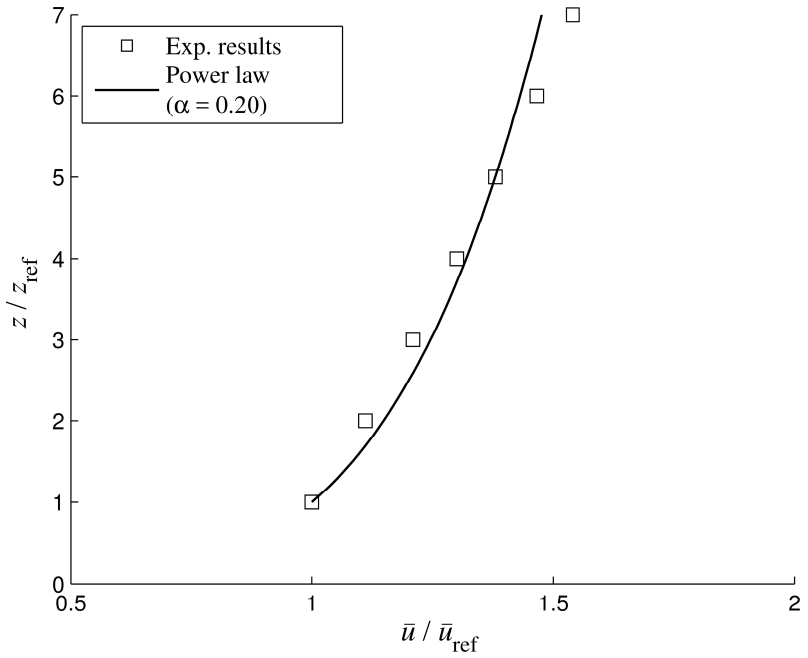

Figure 4.8 Measured mean velocity profile compared to the power law ($\alpha = 0.20$)

A linear-logarithmic presentation of the mean velocity, where the horizontal axis was linear velocity and the vertical axis was height, was compared to the logarithmic law, Figure 4.9, where a very good agreement between the experimental results and the logarithmic law can be observed. The slope of the straight line fitted to the experimental results represents the friction velocity u_τ while the distance on the vertical axis between zero and the intersection of the

straight line represents the aerodynamic surface roughness length z_0. The obtained surface roughness length is $z_{0,m} = 0.003$ m and the friction velocity is $u_\tau = 0.12$ m/s.

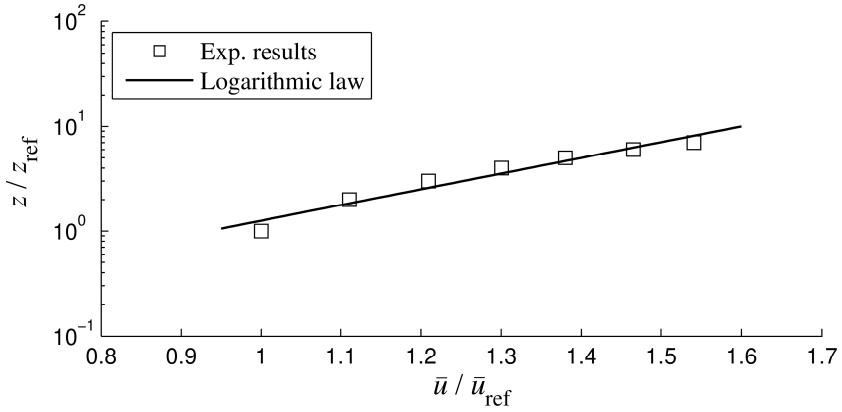

Figure 4.9 Measured mean velocity profile compared to the logarithmic law

4.5.2. Length scale factor for the ABL simulation

Length scale factor for the ABL simulation was calculated using the Cook method [15][15]:

$$S = \frac{91.3\left(z-d\right)^{0.491}}{\left(L_u^{\,x}\right)^{1.403} z_0^{\,0.088}}. \tag{4.2}$$

The scale factors were calculated at x_1 and y_0 in each measurement point in the vertical direction. The final length scale factor was determined as a mean value of scale factors in single points within the useful height range, as described in Kozmar [18]. The ABL simulation length scale factor calculated for this ABL simulation is 1:300.

4.5.3. Turbulence intensity

The experimental results were compared with the international ESDU 85020 [25] standard, Figure 4.10. The heights of the measuring positions in the wind tunnel were scaled-up to full scale using the simulation scale factor of 1:300. The $z_0 = 0.003$ m value determined in the wind tunnel was scaled-up to full scale using the simulation length scale factor 1:300 as well, thus yielding the prototype $z_{0,p} = 0.9$ m. The closest values recommended in ESDU 85020 are for $z_0 = 1$ m and reported with the tolerance margin ±30%. The experimental results are at the lower margin of the reported ESDU 85020 bandwidth.

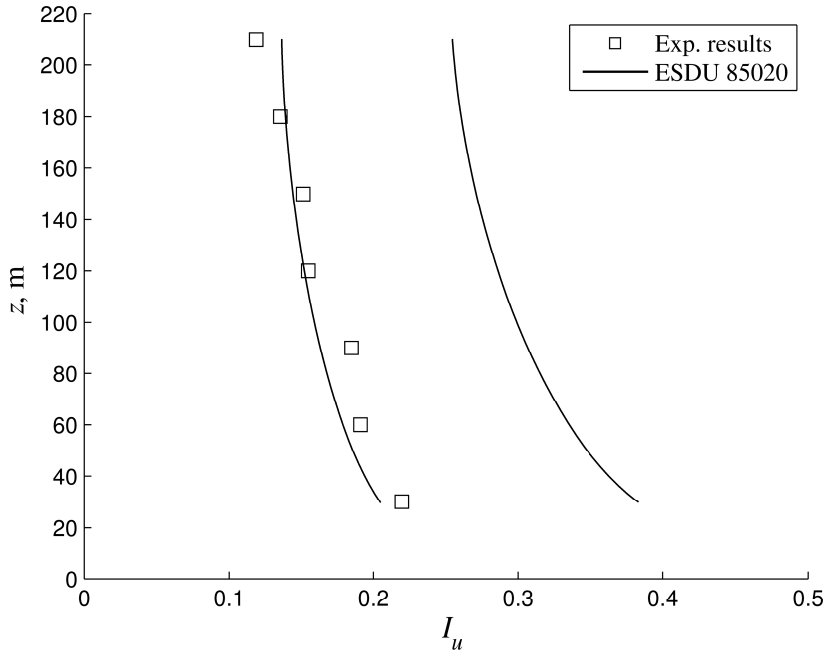

Figure 4.10 Measured turbulence intensity profile compared to ESDU 85020

4.5.4. Turbulent length scales

Measured turbulent length scales were compared with values recommended in the international ESDU 85020 [27] standard for z_0 = 1 m with the tolerance margin ±30%, Figure 4.11. The experimental data does not agree well with the ESDU 85020 data, as the measured turbulent length scales remain constant with increasing height. This is due to an enclosed wind-tunnel test section that prevents large eddies fully to develop, in agreement with previous similar wind-tunnel studies, e.g. Kozmar [26]. This issue is typical for ABL wind-tunnel simulations, as the only limit for eddies in the atmosphere is the Earth surface, while in the wind tunnel they are enclosed both by the wind-tunnel bottom surface, as well as the side walls and the ceiling.

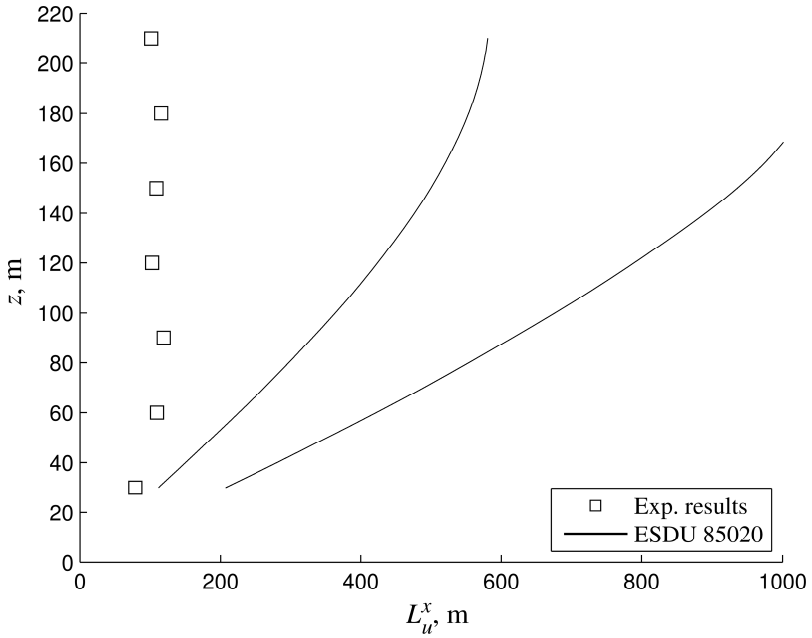

Figure 4.11 Measured turbulent length scales compared to ESDU 85020

4.5.5. Power spectral density of velocity fluctuations

The power spectral density of measured longitudinal velocity fluctuations reported at selected heights (in full-scale measures) presented in Figure 4.12, Figure 4.13, Figure 4.14 and Figure 4.15 compare well with theoretical von Kármán and Kolmogorov models.

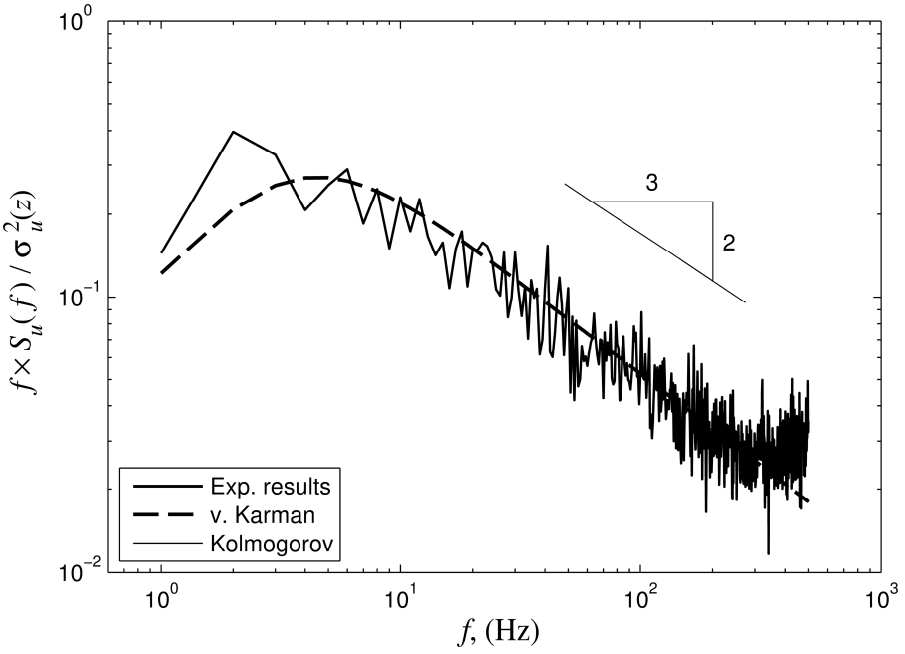

Figure 4.12 Measured power spectral density of velocity fluctuations at z = 30 m (in full-scale measures) compared to von Kármán and Kolmogorov models

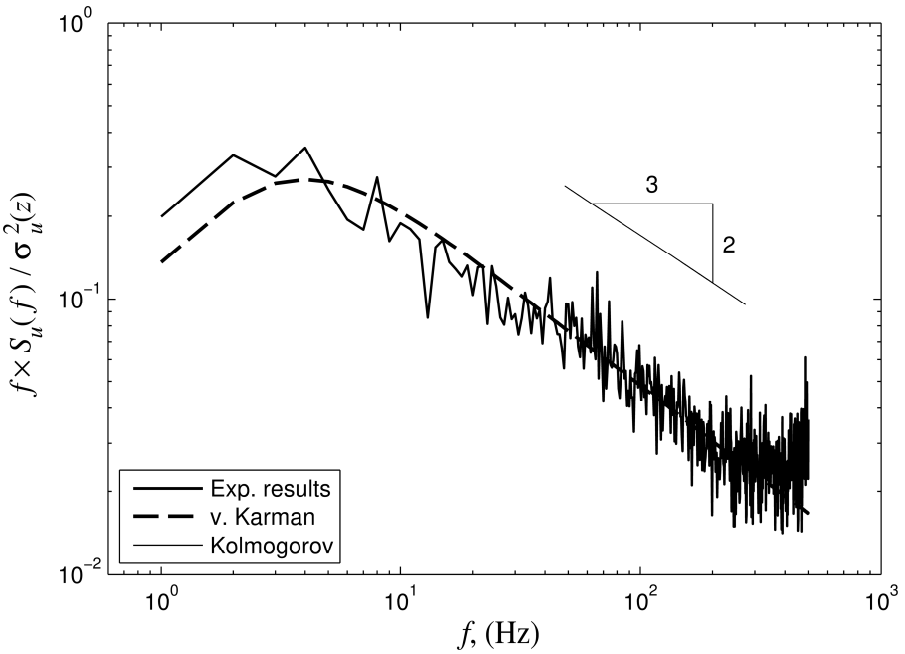

Figure 4.13 Measured power spectral density of velocity fluctuations at z = 90 m (in full-scale measures) compared to von Kármán and Kolmogorov models

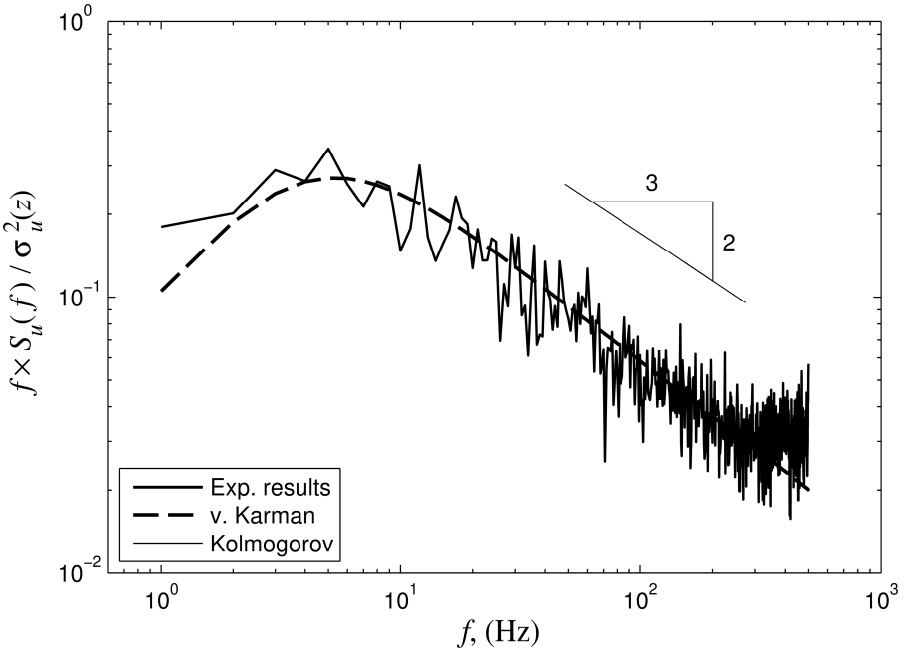

Figure 4.14 Measured power spectral density of velocity fluctuations at z = 150 m (in full-scale measures) compared to von Kármán and Kolmogorov models

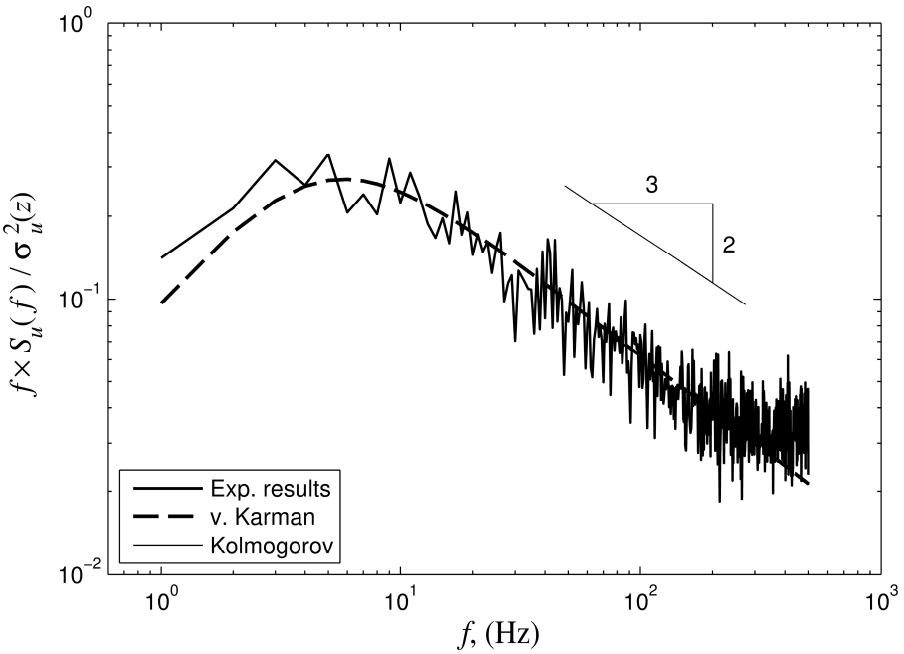

Figure 4.15 Measured power spectral density of velocity fluctuations at z = 210 m (in full-scale measures) compared to von Kármán and Kolmogorov models

5. CONCLUSIONS

Experiments are carried out in the climatic wind tunnel of the Centre of Excellence Telč, Czech Republic, to investigate the influence of castellated barrier wall, vortex generators and surface roughness on flow characteristics and the simulated atmospheric boundary layer. The classical Counihan method was used to experimentally simulate the atmospheric boundary layer. Experimental technique included hot wire, Prandtl-Pitot tube, pressure sensors and thermometers to measure flow velocity, pressure and temperature. Experimental results were reported as profiles of mean flow velocity, turbulence intensity and turbulent length scales, as well as power spectral density of velocity fluctuations, and compared with previous studies, commonly adopted theoretical and empirical laws, international standards and codes. A particular focus was on flow development and uniformity at various positions in the wind-tunnel test section, as well as characteristics of the atmospheric boundary layer simulations at the turntable.

Experimental results indicate a decrease in flow velocity and an increase in turbulence close to the surface due to the castellated barrier wall. Vortex generators enhance turbulence throughout the entire height range under scope. An increased turbulence and a decreased flow are observed close to surface due to surface roughness. The atmospheric boundary layer is successfully simulated for suburban/urban type of terrain. The thickness of the atmospheric boundary simulation is 1.5 m that is approximately equal to the height of vortex generators. The simulation length scale is 1:300, thus yielding the prototype atmospheric boundary layer thickness in the full-scale that is equal 450 m, in agreement with previous relevant studies. Mean velocity profiles are in agreement with the power law characterized with the exponent equal to 0.20, as well as with the logarithmic law. The turbulence intensity profile compares well with the ESDU 85020 data recommended for aerodynamic surface roughness length of 1 m. Turbulent length scales do not compare well with the ESDU 85020 atmospheric data, as the enclosed wind test section prevents large eddies fully to develop, in agreement with previous similar wind-tunnel studies. The power spectral density of velocity fluctuations compares well with the theoretical models of von Kármán and Kolmogorov. Future work would need to further address the three-dimensional aspects of the created ABL simulations.

LITERATURE

[1] Dyrbye, C., Hansen, S.O., Wind loads on structures, John Wiley & Sons, London, 1997.

[2] Kaimal, J.C., Finnigan, J.J., Atmospheric boundary layer flows: their structure and measurement, Oxford University Press, New York, 1994.

[3] Manwell, J.F., McGowan, J.G., Rogers, A.L., Wind energy explained: Theory, design, application, John Wiley & Sons, London, 2009.

[4] Simiu, E., Scanlan, R.H., Wind effects on structures, John Wiley & Sons, 1996.

[5] Kozmar, H., Utjecaj mjerila na strukturu modeliranog atmosferskog graničnog sloja, PhD. Thesis, Zagreb, 2005.

[6] Counihan, J., Adiabatic atmospheric boundary layers: A review and analysis of data from the period 1880-1972, Atmospheric Environment, 9:871-905, 1975.

[7] ESDU, Engineering Sciences Data Unit, 82026, Strong winds in the atmospheric boundary layer, Part 1: Hourly-mean wind speeds, 1982.

[8] ESDU, Engineering Sciences Data Unit, 72026, Characteristics of wind speed in the lower layers of the atmosphere near the ground: strong winds (neutral atmosphere), 1972.

[9] Gromke C., Ruck B., Die Simulation atmosphärischer Grenzschichten in Windkanälen. In: Proceedings of the 13th GALA Fachtagung: Lasermethoden in der Strömungsmesstechnik, Cottbus, Germany, 2005.

[10] Kozmar, H., Physical modeling of complex airflows developing above rural terrains, Environmental Fluid Mechanics, 12:209-225, 2012.

[11] Pernpeintner, A., Lecture notes from course "Aerodynamik der Bauwerke", Lehrstuhl für Fluidmechanik, Fakultät für Maschinenwesen, TU-München, 1998.

[12] Kozmar, H., Modeliranje atmosferskog graničnog sloja u zračnom tunelu, MSc. Thesis, Zagreb, 2000.

[13] Garratt, J.R., The atmospheric boundary layer, Cambridge University Press, 1994.

[14] Pröpper, H., Zur aerodynamischen Belastung großer Kühltürme, Institut für konstruktiven Ingenieurbau, Ruhr-Universität Bochum, Technischwissenschaftliche Mitteilungen, 1977.

[15] Cook, N.J., Determination of the model scale factor in wind tunnel simulations of the adiabatic atmospheric boundary layer, Journal of Wind Engineering and Industrial Aerodynamics, 2:311-321, 1978.

[16] Cermak, J.E., Wind simulation criteria for wind-effect tests, Journal of Structural Engineering, 110:328-339, 1984.

[17] Plate, E.J., Wind tunnel modelling of wind effects in engineering. Engineering meteorology, Elsevier Scientific Publishing Company, 1982.

[18] Kozmar, H., Scale effects in wind tunnel modeling of an urban atmospheric boundary layer, Theoretical and Applied Climatology, 100:153-162, 2010.

[19] Kozmar, H., Wind-tunnel simulations of the suburban ABL and comparison with the international standards, Wind and Structures, 14:15-34, 2011.

[20] Marušić, A., Aerodynamic behavior of bridge cables in icing conditions, MSc. Thesis, Zagreb, 2014.

[21] Plut, M., Experiments on flow and turbulence in the climatic wind tunnel, BSc Thesis, Zagreb, 2013.

[22] Dantec Dynamics, Probes for Hot-wire Anemometry, catalogue, 2015. (http://www.dantecdynamics.com/docs/support-and-download/research-and-education/probepost.pdf)

[23] Jørgensen, F.E., How to measure turbulence with hot-wire anemometers – a practical guide, Dantec Dynamics, 2002.

[24] Wittwer, A. R., Möller, S. V., Characteristics of the low-speed wind tunnel of the UNNE, Journal of Wind Engineering and Industrial Aerodynamics, 84:307-320, 2000.

[25] ESDU, Engineering Sciences Data Unit, 85020, Characteristics of atmospheric turbulence near the ground, Part II: single point data for strong winds (neutral atmosphere), 1985.

[26] Kozmar, H., Characteristics of natural wind simulations in the TUM boundary layer wind tunnel, Theoretical and Applied Climatology, 106:95-104, 2011.